Quaternary Science Reviews 373 (2026) 109728

Contents lists available at ScienceDirect

Quaternary Science Reviews

journal homepage: www.elsevier.com/locate/quascirev

New chronological results from Chaohu Lake Palaeolithic sites in the lower Yangtze River, South China

Shuangwen Yi [a,*,1], Zhe Dong [b,**,1], Shijia Zhan [c], Shuwen Pei [d,e], Huayu Lu [a]

[a] School of Geography and Ocean Science, Nanjing University, Nanjing, 210093, China
[b] Institute of Archaeology and Cultural Relics, Anhui Province, Hefei, 230601, China
[c] School of History and Culture, Liaoning Normal University, Dalian, 116081, China
[d] Institute of Vertebrate Paleontology and Paleoanthropology, Chinese Academy of Sciences, Beijing, 100044, China
[e] Key Scientific Research Base on Paleolithic Human Evolution and Paleogenetics (IVPP), SACH, Beijing, 100044, China

ARTICLE INFO

Handling editor. Christopher Bae

Keywords:
Chaohu Lake region (CLR)
Luminescence dating
Acheulean large tools
Lithic miniaturization
South China

ABSTRACT

Systematic field investigations and excavations in the lower Yangtze River region have uncovered numerous open-air Palaeolithic sites, yielding a wealth of stone artifacts crucial for understanding lithic technological evolution and hominin adaptive behaviors during the Middle to Late Pleistocene in South China. However, chronological frameworks and technological patterns in this region remain underexplored. This study applies multiple luminescence dating techniques to establish precise age estimates for three Palaeolithic sites in the Chaohu Lake region of Anhui Province, South China. Our high-resolution geochronological results indicate site occupation from approximately 200 to 30 ka. The lower archaeological unit, containing large scrapers, cleavers, and handaxes, dates to 200–70 ka, marking the emergence of a Large Cutting Tool techno-complex during MIS 5, possibly extending into MIS 6 or 7. In contrast, the upper archaeological unit, dated to 60–30 ka, is dominated by small flakes and flaked tools, reflecting the development of lithic miniaturization and an increased reliance on high-quality raw materials during MIS 3. These findings reveal a technological shift from Acheulean large flake technology to the dominance of miniaturized flake tools from the late Middle Pleistocene to the Late Pleistocene, closely linked to environmental and ecological changes in South China.

1. Introduction

The emergence and dispersal patterns of modern humans in East Asia have recently become a pivotal research focus in paleoanthropology, driven by a growing number of discoveries that reveal the extensive spatial and temporal distribution of early human remains (Bae, 2017, 2024). In southern China, systematic investigations of numerous open-air Palaeolithic sites and cave systems dated to the Middle–Late Pleistocene have yielded substantial evidence for understanding early human behavior (Liu et al., 2010, 2015; Bae et al., 2014; Martinon-Torres et al., 2021; Sun et al., 2021). Particularly significant are the cave sites in the region that have yielded potential evidence of human occupation during the early Late Pleistocene (~130–70 ka), corresponding to Marine Isotope Stage (MIS) 5, offering crucial chronological markers for modeling early dispersal dynamics (Liu et al., 2010, 2015; Fu et al., 2013; Bae et al., 2017). These findings underscore the importance of southern China in elucidating the evolutionary trajectory of modern humans (Liu et al., 2010, 2015; Gao et al., 2017; Wu et al., 2019; Bae, 2024). Nevertheless, this trajectory remains poorly defined due to the scarcity of well-preserved human fossils and unresolved chronological frameworks, often arising from ambiguous stratigraphic contexts and uncertain associations (Sun et al., 2021; Hublin, 2021; Ge et al., 2024).

In addition to cave records, extensive open-air Palaeolithic sites across South China—particularly in the lower Yangtze River region—provide crucial complementary evidence of hominin activity (Fang, 1997, 2002; Fang et al., 2003; Zhang et al., 2003, 2004; Xu, 2008; Dong et al., 2019; Li, 2020; Li et al., 2022; Zhan et al., 2025). Stone artifacts recovered from these contexts offer valuable insights into lithic technological development and hominin adaptive strategies during the

* Corresponding author.
** Corresponding author.
E-mail addresses: ysw7563@nju.edu.cn (S. Yi), jludongzhe@sina.com (Z. Dong).
[1] These authors are co-first authors.

https://doi.org/10.1016/j.quascirev.2025.109728
Received 9 July 2025; Received in revised form 6 November 2025; Accepted 24 November 2025
Available online 2 December 2025

Middle to Late Pleistocene (Wang et al., 2012; Xie et al., 2020). However, the classification of these lithic industries remains contentious. Some scholars categorize them as part of a Pebble Tool Industry (Oldowan-like, Mode 1), based on the absence of typical Mode 2 (Acheulean) traits (Schick, 1994; Gao, 2013; Guan et al., 2018). Conversely, others argue for the presence of Mode 2 or Acheulean-like technology, citing the presence of large cutting tools (LCTs), such as handaxes, systematic exploitation of large cores, and the production of morphologically standardized large flakes since the Middle Pleistocene (Wang et al., 2014; Li et al., 2018, 2022, 2024; Dong et al., 2019; Zhan et al., 2025). This typological controversy is further complicated by the marked scarcity of securely dated sites from the late Middle to early Late Pleistocene—a critical period corresponding to the emergence of modern humans in South China—thereby limiting our understanding of the lithic cultural context associated with these populations (Bae et al., 2018; Xie et al., 2020; Wang, 2024).

Notable archaeological evidence has emerged since the 1980s from the Chaohu Lake Region (CLR) (Xu et al., 1984, 1986; Fang, 1990; Fang and Han, 1993; Zhan et al., 2022, 2025; Dong, 2025a) and the Shuiyangjiang River Basin (Fang, 1988, 1997; Fang et al., 2001; Dong et al., 2019; Dong and Zhan, 2020, 2022; Zhan and Dong, 2023; Dong, 2025b) in Anhui Province, central South China. These regions have yielded both human fossils and stone artifacts, often embedded within Quaternary Red Clay (QRC) deposits, indicating long-term hominin occupation. Technological analyses reveal the systematic production of large flakes from sizable cores and the manufacture of LCTs, supporting the presence of Mode 2 technological behaviors in the lower Yangtze River region (Li et al., 2021, 2024). By the Late Pleistocene, lithic technology in these areas underwent substantial reorganization, marked by the use of high-quality raw materials, tool miniaturization, and the emergence of composite tools—highlighting the region's importance in tracing technological trajectories in subtropical East Asia (Zhan et al., 2025). However, precise interpretation remains constrained by a lack of securely dated contexts, underscoring the need for integrated studies that combine high-resolution stratigraphy, advanced dating techniques, and paleoenvironmental reconstruction.

In this regard, optically stimulated luminescence (OSL) dating has emerged as a robust method for establishing absolute chronologies of archaeological sediments worldwide (Roberts et al., 2015; Jacobs et al., 2019). While quartz-based OSL using the single-aliquot regeneration (SAR) protocol is widely adopted, its effectiveness is limited by signal saturation at relatively low doses (~200 Gy), restricting its applicability to the last ~100 ka (Murray et al., 2021). To address this limitation, extended-range luminescence techniques have been developed, including thermally transferred OSL (TT-OSL) of quartz (TT-OSL; Wang et al., 2006a, b; Tsukamoto et al., 2008; Porat et al., 2009; Stevens et al., 2009; Adamiec et al., 2010) and post-infrared infrared stimulated luminescence (pIRIR) dating of K-feldspars (Thiel et al., 2011; Buylaert et al., 2012; Li and Li, 2011, 2012). These methods exhibit higher dose saturation limits and have been increasingly applied to Middle and Late Pleistocene sites in China, including those with complex stratigraphy such as QRC deposits (Sun et al., 2021; Li et al., 2022).

This study aims to establish a refined chronological framework for Paleolithic sites in the CLR using a multi-method luminescence approach, including quartz SAR-OSL, TT-OSL, and K-feldspar pIRIR ($pIR_{50}IR_{225}$ and $pIR_{200}IR_{290}$) dating. By integrating luminescence chronologies with stratigraphic, sedimentological (e.g., grain size, magnetic susceptibility), and geochemical proxies (e.g., stable carbon isotopes, major elemental composition), we seek to reconstruct the paleoenvironmental context of hominin occupations. Furthermore, through comparative analysis of lithic assemblages within a regional techno-typological framework, this research investigates early human adaptive strategies in response to local environmental changes. Ultimately, the results contribute to a deeper understanding of early human dispersals and technological adaptations in South China.

2. Geographic and archaeological settings

The Chaohu Lake Region (CLR), situated in the lower reaches of the Yangtze River (Fig. 1), is characterized by extensive QRC deposits that overlie Tertiary peneplains and river terraces (Zhao and Yang, 1995; Xiong et al., 2002; Hu et al., 2003). The region experiences a humid subtropical monsoon climate, marked by distinct seasonal contrasts between summer and winter monsoons, with mean annual precipitation ranging from 1000 to 1600 mm and average temperatures between 16 and 18 °C. These climatic conditions support a vegetation landscape dominated by deciduous oak forests interspersed with evergreen species (Wang, 2022).

Open-air Palaeolithic sites in the CLR were first documented in 1988, yielding numerous lithic artifacts from both surface and QRC contexts (Fang, 1990). Subsequent excavations in 1991 expanded the artifact assemblage but did not include chronometric dating, leading to a tentative Middle–Late Pleistocene attribution based on techno-stratigraphic correlations (Fang and Han, 1993). Recent investigations in 2019 by the Institute of Archaeology and Cultural Relics of Anhui Province identified 16 new Palaeolithic localities and one fossil site within 5 km of the Chaoxian Man Site in Chaohu City (Fig. 1). These localities yielded a total of 939 stone artifacts and fragmentary faunal remains, recovered either *in situ* or from surface contexts on the second and third fluvial terraces (Fig. 2). Among the lithic assemblage, 16 LCTs were identified, including three handaxes, seven knives, two cleavers, three picks, and one preform. Additionally, several miniaturized flaked tools manufactured from black rhyolitic tuff were found at one locality. The presence of such diverse tool types suggests that the localities represent different cultural periods (Zhan et al., 2022).

This study focuses on three representative Palaeolithic sites—Zhangjiawan (ZJW), Wangchenggang (WCG), and Liujia 2 (LJ2)—shown in Fig. 1 and Fig. S1. While ZJW and WCG are naturally exposed sections, LJ2 was systematically excavated in 2021, yielding 1124 *in situ* artifacts (Dong, 2025a). The assemblage includes manuports, cores, flakes, debitage, utilised materials (unmodified items with functional edge-wear), and retouched stone tools (Fig. S1, Table S1). Due to its well-preserved stratigraphy and abundance of artifacts, LJ2 serves as the primary stratigraphic reference in this study. A detailed comparison of the stratigraphic sequences across the three sites is provided in the following section.

1) Zhangjiawan (ZJW, 31°34′27"N; 117°47′47"E)

The ZJW site is a naturally exposed section along a gently sloping road, with a total thickness of approximately 5 m (Fig. S1A). The stratigraphy is divided into four layers: Layer 1 (0–0.2 m): cultivated topsoil with a loose structure, clay coatings, and abundant organic matter. Layer 2 (0.2–2.0 m): homogeneous red-brown soil with an angular blocky structure and minor dark films indicative of iron–manganese eluviation. Layer 3 (2.0–4.0 m): red-brown soil with a pronounced net-like structure, sporadic white specks, and short white veins. Layer 4 (4.0–5.0 m): sand and gravel composed primarily of poorly sorted siltstone, quartz sandstone, and quartzite (Fig. 2).

Lithic artifacts at ZJW are stratigraphically distributed within Layers 2 and 3 (0.2–4.0 m). Surface surveys recovered only two diagnostic artifacts, both made of quartzite: one polyhedron and one heavy-duty scraper (Zhan et al., 2022). However, lithic debitage has been systematically recorded throughout the sedimentary sequence.

2) Wangchenggang (WCG, 31°34′12"N; 117°50′59"E)

The WCG site represents a residual accumulation of QRC with a total thickness of approximately 1.0 m (Fig. S1B).

Early archaeological investigations conducted during the 1980s–1990s were limited by the absence of systematic spatial documentation, resulting in incomplete contextual information regarding

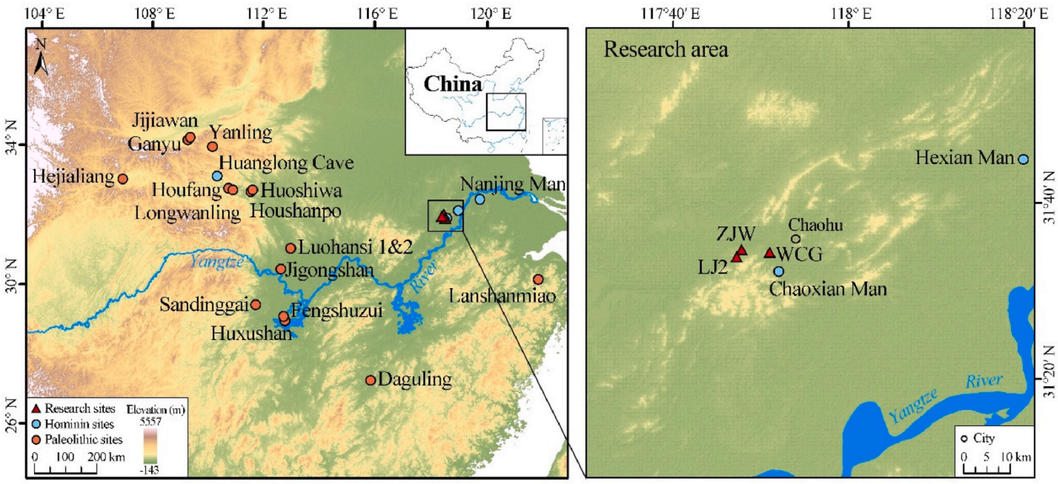

Fig. 1. Geographic locations of study sites (red triangles) and Palaeolithic/hominin sites mentioned in the main text. Jijiawan (Wang et al., 2014a; Zhuo et al., 2016); Ganyu (Wang et al., 2014a; Zhuo et al., 2016), Yanling (Li et al., 2023); Hejialiang (Sun et al., 2012; Wang et al., 2014b); Houfang (Li et al., 2018a, 2018b); Longwanling (Guo et al., 2025); Lanshanmiao (Lu et al., 2020), Daguling (Fang et al., 2003), Houshanpo (Guo et al., 2021), Huoshiwa (Guo et al., 2021), Luohansi 1 (Yan et al., 2024), Luohansi 2 (Yan et al., 2024), Jigongshan (Guo et al., 2020), Fengshuzui (Zhang et al., 2019), Huxushan (Lai et al., 2021a), and Sandinggai (Li et al., 2022), Hexian Man (Huang et al., 1981, 1982), Chaoxian Man (Xu et al., 1984, 1986), Nanjing Man (Zhao et al., 2001), and Hualongdong Cave (Wu et al., 2019). (For interpretation of the references to colour in this figure legend, the reader is referred to the Web version of this article.)

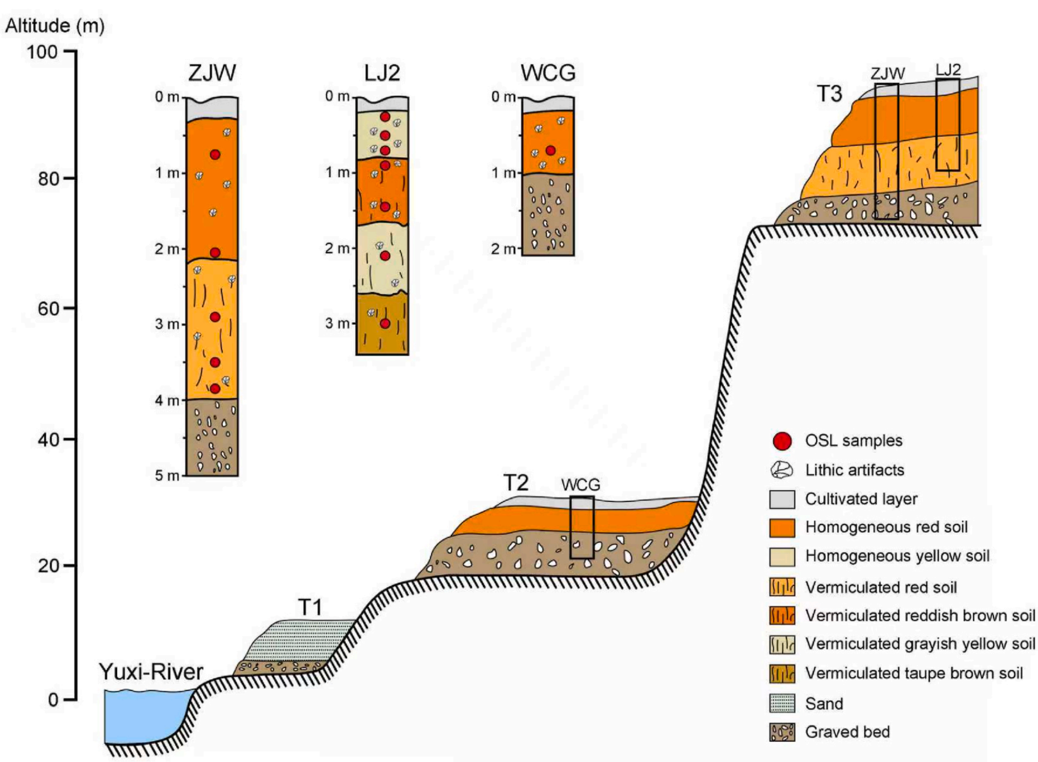

Fig. 2. Geomorphology and pedostratigraphy of Palaeolithic sites in the Chaohu Lake region (CLR), showing the second and third terraces of an ancient river.

lithic provenance. However, recent reanalysis of the artifact assemblage has revealed a well-defined *chaîne opératoire* indicative of Acheulean large flake production and shaping. The lithic assemblage includes cores, flakes, debitage, utilised materials, and retouched tools. Quartzite is the dominant raw material (97.5 %), followed by quartz (2.2 %) and basalt (0.3 %). The artifacts range from medium to large in size, with average dimensions of 87.45 mm in length, 74.89 mm in width, and 49.62 mm in thickness. Typological analysis identifies characteristic Acheulean elements, including bifacial handaxes, cleavers, and knives, as well as massive scrapers and denticulates (Zhan et al., 2025).

3) Liujia 2 (LJ2, 31°33′39.93"N; 117°47′17.87"E)

The LJ2 site comprises two excavation areas (Zone I and Zone II), with the studied profile located in Excavation Area I. This newly excavated trench reaches a depth of 3.4 m (Fig. S1C and S1D) and is subdivided into five pedostratigraphic units, distinguished by variations in colour, texture, and the presence of white net-like veins (Fig. 2). Layer 1

(0–0.2 m): loose, cultivated topsoil rich in organic material. Layer 2 (0.2–0.8 m): homogeneous yellow clay loam with sporadic light-coloured spots and fine, short white veins. Layer 3 (0.8–1.7 m): red-brown clay loam with a prominent net-like structure and numerous short white veins. Layer 4 (1.7–2.6 m): grey-yellow clay loam featuring abundant net-like patterns and short white veins. Layer 5 (2.6–3.4 m): grey-brown clay loam, also characterised by abundant white veining and net-like patterns. These pedological features are indicative of aquic soil conditions resulting from alternating anaerobic and aerobic environments.

The lithic assemblage at LJ2 includes manuports, cores, flakes, debitage, utilised materials, and retouched tools. While artifacts are distributed throughout Layers 2 to 5 (0.2–3.4 m), they are heavily concentrated in Layer 2 (0.2–0.6 m) (Fig. S2). Field observations and typological analysis support the division of the assemblage into two Archaeo-stratigraphic Units (AUs) (Dong, 2025a). The upper AU (Layer 2, 0.2–0.6 m), a 0.4 m-thick unit yielded 771 artifacts, predominantly light-duty tools such as scrapers, notches, denticulates, and burins. Black rhyolitic tuff is the most common raw material (49.3 %), followed by quartz (22.4 %), quartzite (22.2 %), and quartz sandstone (5.8 %). Artifacts made of rhyolitic tuff and quartz are relatively small, with average maximum lengths of 25.97 mm and 25.81 mm, respectively, whereas those made from quartzite and quartz sandstone are larger, averaging 45.85 mm and 47.92 mm. The lower AU (Layers 3–5: 0.6–3.4 m), a 2.8 m sequence, produced 353 artifacts, predominantly made of quartzite (56.7 %) and quartz sandstone (30.0 %), with minor components of quartz (9.6 %), rhyolitic tuff (3.1 %), and granite (0.6 %). The assemblage is characterised by larger artifacts (average length: 45.8 mm), including 20 specimens exceeding 100 mm in length, and features typical Acheulean LCTs such as knives and cleavers, along with massive scrapers and denticulates (Fig. 3; Table S1).

3. Materials and methods

3.1. Sampling

A total of thirteen OSL samples were collected from the three Palaeolithic sites using light-tight stainless steel cylinders (5 cm in diameter and 25 cm in length). The distribution of sampling varied by site: five samples were taken from the ZJW profile at depths of 0.75,

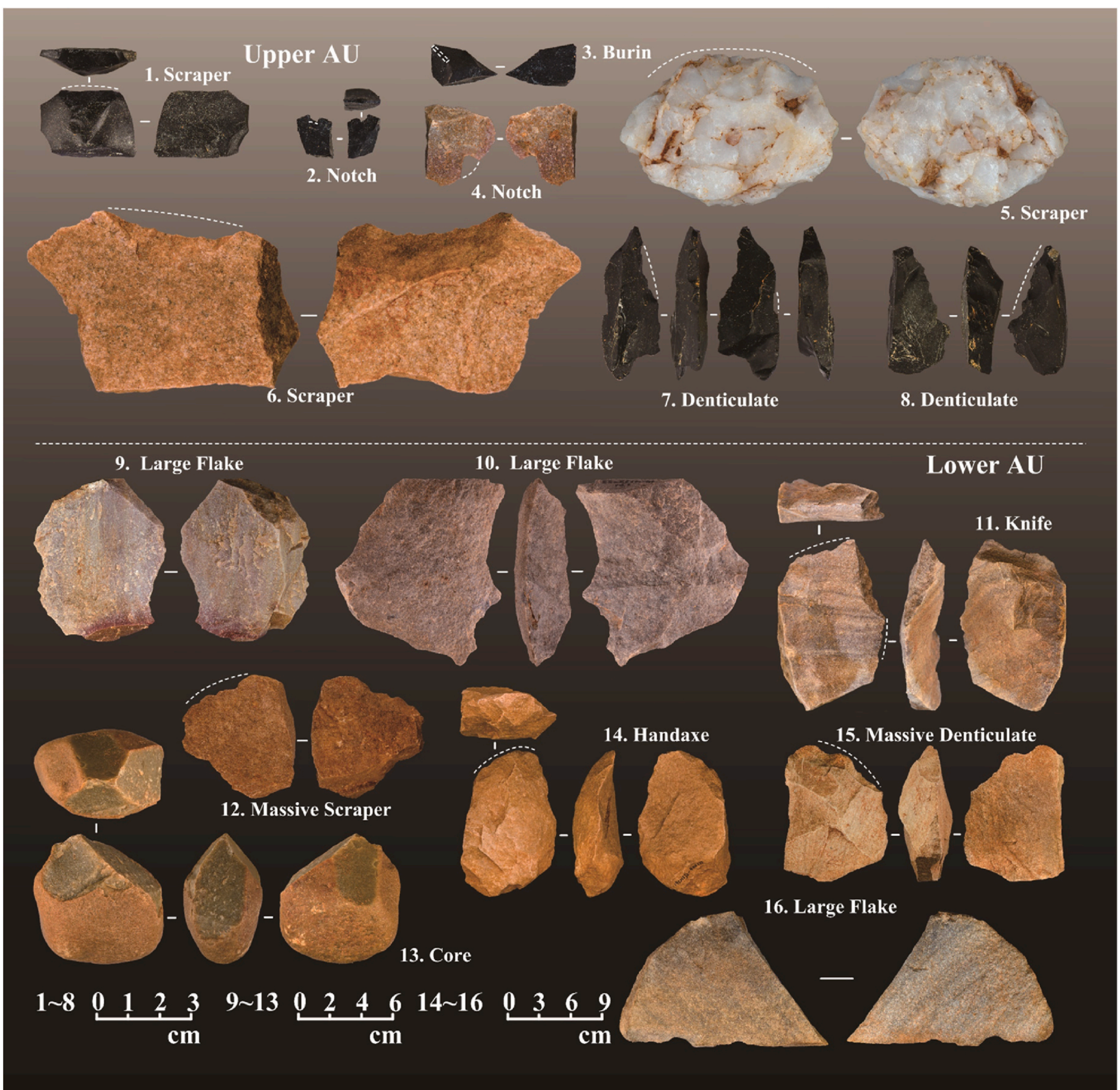

Fig. 3. Lithic assemblages discovered from different Archaeo-stratigraphic Units (AU) in the Liujia 2 (LJ2) site (miniaturized flake tools buried in the upper AU; lower AU contained Acheulean products).

2.05, 2.9, 3.5, and 3.85 m; one sample was obtained from the WCG profile at 0.70 m; and seven samples were systematically extracted from the LJ2 section at depths of 0.25, 0.50, 0.70, 0.90, 1.45, 2.10, and 3.00 m. In addition, 76 bulk sediment samples were collected at 10 cm intervals from the excavated LJ2 profile to facilitate high-resolution stratigraphic correlation through multi-proxy analyses, including grain size, magnetic susceptibility, and geochemical measurements.

3.2. Luminescence dating

All luminescence samples were processed under subdued red-light conditions at the Luminescence Dating Laboratory, Nanjing University. The outer 2–5 cm of each sample cylinder was reserved for water content and dosimetry analysis, while the inner portion was used for dating. The inner sediment was treated with 30 % hydrochloric acid (HCL) and 30 % hydrogen peroxide (H_2O_2) to remove carbonates and organic matter, following wet sieving. For the ZJW and WCG sites, coarse-grained quartz (63–90 μm) was extracted through heavy liquid separation and etched with hydrofluoric acid. At the LJ2 site, fine-grained quartz (4–11 μm) was isolated by settling according to Stokes' Law and then purified with 30 % hydrofluorosilicic acid (H_2SiF_6) for one week. The purity of all quartz extracts was confirmed using the OSL–IR depletion ratio test (Duller, 2003). Polymineral fine grains (4–11 μm) from all three sites were also prepared for K-feldspar measurements.

Luminescence signals were measured using a Risø TL/OSL-20 automated reader equipped with blue (470 nm, ~80 mW/cm^2) and infrared (870 nm, ~135 mW/cm^2) LED units. Both coarse quartz and fine grains were mounted as large aliquots (~8 mm); coarse grains were adhered to stainless-steel discs with silicone spray. Quartz OSL signals were detected through a 7.5-mm-thick Schott U-340 filter, while infrared-stimulated luminescence (IRSL) signals were filtered using a combination of Corning 7–59 and Schott BG-39 filters.

Equivalent doses (D_e) were determined using four protocols (Table S2). Quartz grains were dated using both the standard SAR-OSL protocol (Table S2a; Murray and Wintle, 2003) and the TT-OSL protocol (Table S2b; Stevens et al., 2009). In the SAR-OSL protocol, a preheat of 260 °C and a cutheat of 220 °C were applied, and the OSL signal was stimulated at 125 °C for 40 s. An IR stimulation at room temperature was included prior to the final OSL measurement to monitor feldspar contamination (Duller, 2003). The net OSL signal was derived from the first 0.16 s of stimulation, with an early background subtraction (0.16–0.32 s), to reduce the contribution of slow and medium components (Cunningham and Wallinga, 2010). For TT-OSL, two preheats of 260 °C for 10 s were applied before measuring the natural signal. Sensitivity changes were monitored via the response of the TT-OSL signal to a test dose. To remove residual signals from previous dosing steps, two high-temperature (280 °C) blue-light stimulations were introduced mid-cycle and at the end of each SAR cycle (Table S2b; Stevens et al., 2009). K-feldspar grains were dated using two post-IR IRSL protocols (Table S2c and d; Thiel et al., 2011; Buylaert et al., 2009, 2012; Li and Li, 2012). The $pIRIR_{290}$ protocol (i.e. $pIR_{200}IR_{290}$, Table S2c) involved a 320 °C preheat (60 s), IR stimulation at 200 °C, and pIRIR stimulation at 290 °C. The $pIRIR_{225}$ protocol (i.e. $pIR_{50}IR_{225}$, Table S2d) employed a 250 °C preheat and pIRIR stimulation at 225 °C. For both feldspar signals, D_e was calculated from the initial 2 s of the pIRIR signal after subtracting the last 50 s as background.

A dose recovery test was conducted using a younger sample (NJU4005, ~120 Gy) to assess the accuracy of the SAR protocol (Wallinga et al., 2000; Murray and Wintle, 2003). For standard quartz OSL, six natural aliquots were bleached twice with blue light at 125 °C for 60 s each and then given a laboratory dose close to the natural D_e. For quartz TT-OSL and K-feldspar pIRIR signals ($pIR_{200}IR_{290}$ and $pIR_{50}IR_{225}$), varying laboratory doses were administered to circumvent potential complications from incomplete bleaching (SARA, Mejdahl and Bøtter-Jensen, 1994; Wallinga et al., 2001).

The quartz TT-OSL signal is known to bleach more slowly than conventional OSL (Wang et al., 2006b; Tsukamoto et al., 2008). Similarly, high-temperature pIRIR signals (e.g., $pIR_{200}IR_{290}$) bleach more slowly than lower-temperature IRSL signals (Buylaert et al., 2012; Kars et al., 2014; Yi et al., 2016). To examine the bleachability of these signals, 15 aliquots were exposed to a Hönle SOL2 solar simulator for 40–300 h, targeting TT-OSL and $pIR_{200}IR_{290}$ signal reduction.

The lower-temperature pIRIR signal ($pIR_{50}IR_{225}$) is expected to bleach more readily than its high-temperature counterpart ($pIR_{200}IR_{290}$), potentially reducing the risk of age overestimation (Lowick et al., 2012; Colarossi et al., 2015). However, it is susceptible to anomalous fading, which can lead to D_e underestimation (Spooner, 1994; Huntley and Lamothe, 2001; Huntley and Lian, 2006). To evaluate the stability of this signal, an anomalous fading test was conducted, and *g*-values were determined for twelve aliquots following Auclair et al. (2003).

The environmental dose rates were derived from measurements of uranium (U), thorium (Th), and potassium (K) concentrations. For the ZJW and WCG samples, elemental concentrations were determined using a combination of inductively coupled plasma mass spectrometry (ICP-MS) and optical emission spectrometry (ICP-OES). For the LJ2 samples, high-resolution gamma spectrometry was employed following the method of Murray et al. (1987). Prior to analysis, samples were sealed for four weeks to ensure secular equilibrium, and gamma counting was performed under low-background conditions for durations exceeding 24 h.

Water content was estimated based on the mass difference between wet and oven-dried samples. Most LJ2 samples exhibited water contents below 10 %, likely reflecting post-excavation drying effects due to prolonged exposure. However, given the high mean annual precipitation in the region (1000–1600 mm), these values were considered unrepresentative of actual burial conditions. Therefore, a notional water content of 20 ± 10 % was adopted for LJ2, consistent with values reported from other Palaeolithic sites in comparable climatic settings (Zhang et al., 2019; Lai et al., 2021a; Li et al., 2022). Dose rates for fine-grained quartz and the polymineral fraction were calculated using α-efficiency values of 0.04 ± 0.02 (Rees-Jones, 1995) and 0.010 ± 0.014 (Schmidt et al., 2018), respectively. For K-feldspar, a potassium concentration of 12.5 ± 0.5 % (Huntley and Baril, 1997) and a rubidium content of 400 ± 100 ppm (Huntley and Hancock, 2001) were assumed. The cosmic dose rate was estimated following the method proposed by Prescott and Hutton (1994). Finally, elemental concentrations were converted to effective dose rates using the dose conversion factors of Guérin et al. (2011), incorporating attenuation due to water content following Aitken (1985).

3.3. Climate proxy analysis

Grain-size distributions (GSDs) were measured using a Malvern Mastersizer 2000 laser particle size analyzer (measurement range: 0.02–2000 μm; relative error: <2 %). Prior to analysis, all samples underwent complete pre-treatment to disaggregate particle aggregates, following the protocol of Lu and An (1997). To deconvolve sediment sources and transport mechanisms, the measured GSDs were subjected to end-member mixing analysis (EMMA). This method identifies the minimum number of statistically significant end-members by optimizing the coefficient of determination (R^2) and minimizing the mean angular deviation (θ). A robust model fit is typically indicated by R^2 values exceeding 0.9 and θ values below 5° (Paterson and Heslop, 2015).

Low-frequency magnetic susceptibility (MS) was measured at 0.47 kHz using a Bartington MS2 meter. Approximately 10 g of dried sediment from each sample was measured in triplicate, and results were normalized by mass to yield mass-specific MS values.

Major element concentrations were determined using a Thermo Scientific ARL 9900 X-ray fluorescence (XRF) spectrometer. Prepared samples were oven-dried, ground to 200 mesh under standardised conditions, and compacted into round discs for analysis. Analytical uncertainties were typically within ±2 % for most major elements, except for P_2O_5 and MnO, which had uncertainties below ±10 %. Weathering intensity was assessed using the Chemical Index of Alteration (CIA; Nesbitt and Young, 1982) and the Weathering Index of Parker (WIP; Parker, 1970), in line with established protocols for analyzing QRC sediments from Palaeolithic contexts in southern China (Zhang et al., 2019).

The stable carbon isotopic composition of organic matter ($\delta^{13}C_{org}$) was analyzed using a Thermo Flash 2000 HT Elemental Analyzer coupled to a MAT-253 Plus isotope ratio mass spectrometer. Sample preparation involved oven-drying at 45 °C for 48 h, sieving to <50 mesh to remove visible plant debris, and grinding to a fine powder of 200 mesh. Carbonates were removed by treatment with 2 mol/L HCl, followed by repeated rinsing with distilled water until a neutral pH (~7) was reached. Samples were then redried at 45 °C. The analytical precision, based on the standard deviation of replicate measurements, was better than ±0.1 ‰.

4. Results

4.1. Dating results

Representative signal decay curves and dose response curves (DRCs) are shown in Fig. 4. The quartz OSL signal exhibits rapid decay within the first second of stimulation (Fig. 4A), confirming the dominance of the fast component (Singarayer and Bailey, 2003). Most quartz DRCs approach a saturation plateau, with natural signal intensities reaching or exceeding 85 % of the saturation level (defined by $2D_0$; Wintle and Murray, 2006), resulting in measured D_e values of ≥200 Gy. In contrast, the TT-OSL and K-feldspar pIRIR signals ($pIR_{50}IR_{225}$ and $pIR_{200}IR_{290}$) display substantially higher saturation limits (Fig. 4B–D), underscoring their suitability for dating older deposits. Notably, while K-feldspar signals from deeper stratigraphic units approached saturation, the TT-OSL DRCs remained nearly linear and below ~85 % saturation, indicating a higher dose capacity.

Dose recovery tests for quartz SAR-OSL yielded a ratio of 1.05 ± 0.01 using a preheat of 260 °C and a cut-heat of 220 °C settings. For K-feldspar $pIR_{200}IR_{290}$, acceptable dose recovery (within 10 % of unity) was maintained up to ~600 Gy, beyond which the recovery ratios began to diverge (Fig. 5). The $pIR_{50}IR_{225}$ signal yielded a recovery ratio of 1.09 ± 0.03 for a 600 Gy dose, while quartz TT-OSL produced a ratio of 0.92 ± 0.01 for a 684 Gy dose. These results collectively confirm the reliability of the applied measurement protocols.

The $pIR_{200}IR_{290}$ signal decreased to a residual dose of 6 ± 1 Gy after 40 h of bleaching under a solar simulator and stabilized thereafter (Fig. 6A), consistent with previous findings from aeolian loess (Yi et al., 2016, 2018, 2022). The TT-OSL signal, however, showed greater bleaching resistance, retaining a residual dose of 19 ± 1 Gy even after 300 h of exposure (Fig. 6A), in line with its known slow-bleaching behavior (Wang et al., 2006b; Tsukamoto et al., 2008; Liu et al., 2016). These residual doses were subtracted from the corresponding D_e values prior to age calculation.

Anomalous fading measurements for the $pIR_{50}IR_{225}$ signal yielded a $g_2$days value of 1.21 ± 0.14 %/decade, significantly lower than that of the IR_{50} signal (2.01 ± 0.09 %/decade; Fig. 6B). This result is consistent with previously values (~1.5 ± 0.1 %/decade; Li et al., 2014), and given its low magnitude (<~1.5 %/decade), no fading correction was applied.

Radionuclide concentrations and total dose rates show no systematic variation with depth across the stratigraphic sequences, suggesting relatively homogeneous depositional conditions and post-depositional stability (Fig. 8; Table S3). Uranium concentrations remain relatively constant with depth, and U/Th ratios range from 0.21 to 0.28 (Fig. 8). These values are comparable to those reported for red clay at Palaeolithic sites in Hunan (0.20–0.22; Zhang et al., 2019; Li et al., 2022) and Fujian (0.22–0.29; Jin et al., 2023), but significantly higher than those observed in Late Pleistocene red sands from coastal southern Fujian (0.15–0.16; Zhang et al., 2008; Jin et al., 2018).

The resulting D_e values and corresponding ages are summarized in Fig. 7 and Table 1. At the LJ2 site, quartz SAR-OSL ages range from 31.6

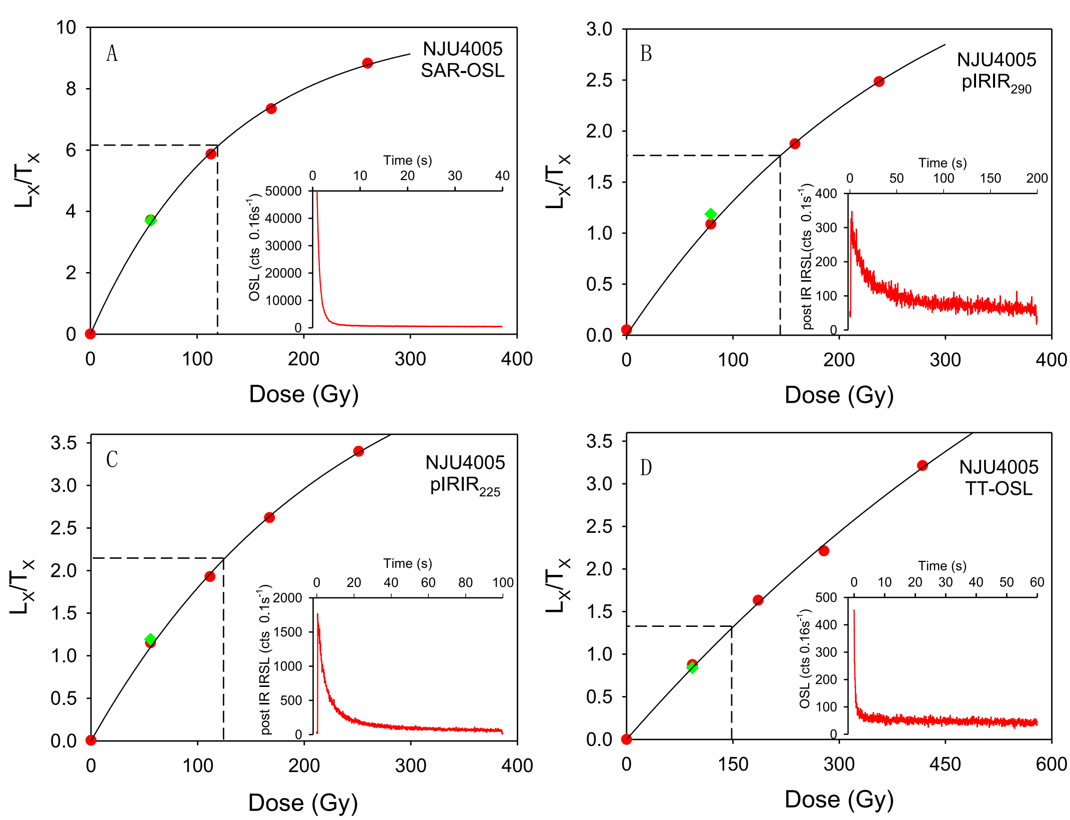

Fig. 4. Typical dose response curves for aliquots of samples derived from different signals (inset shows the natural decay curves).

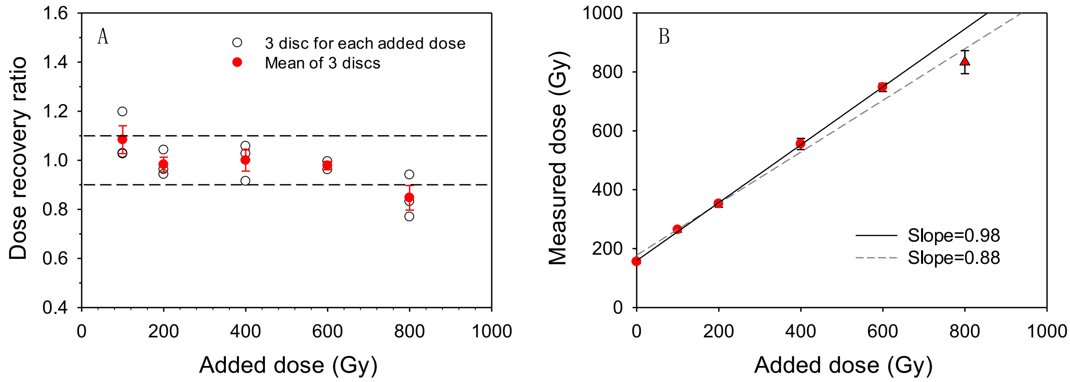

Fig. 5. Results of the feldspar $pIR_{200}IR_{290}$ dose recovery tests. The experiment involved adding different laboratory doses on top of a natural sample. (B) Data in (A) are shown as the measured dose versus the added dose. The open circles indicate three different aliquots at each dose, and red filled circles show the average of the three aliquots. (For interpretation of the references to colour in this figure legend, the reader is referred to the Web version of this article.)

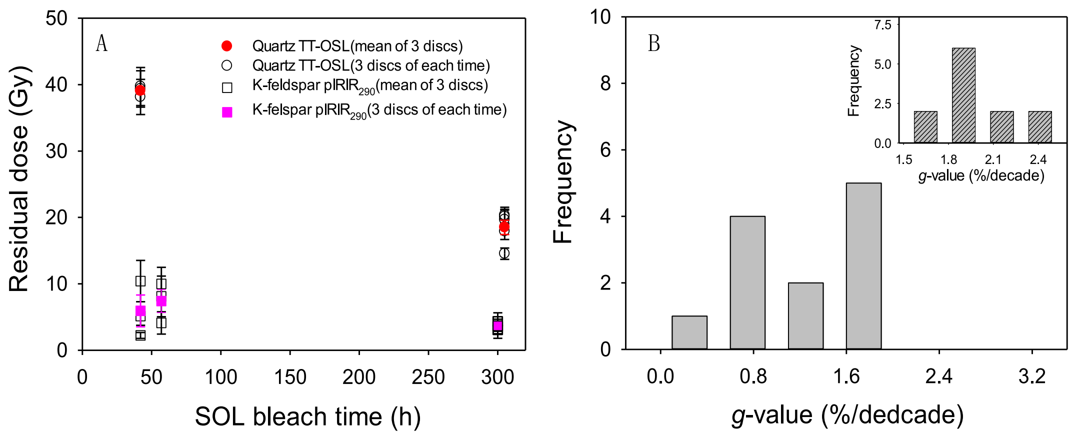

Fig. 6. A) Comparison of residual doses for quartz TT-OSL and K-feldspar $pIR_{200}IR_{290}$ signals after bleaching with Hönle SOL2 solar simulator; B) Fading rate (*g*-value) determination of K-feldspar $pIR_{50}IR_{255}$ signals. The inset shows the *g*-value of IR_{50} signals.

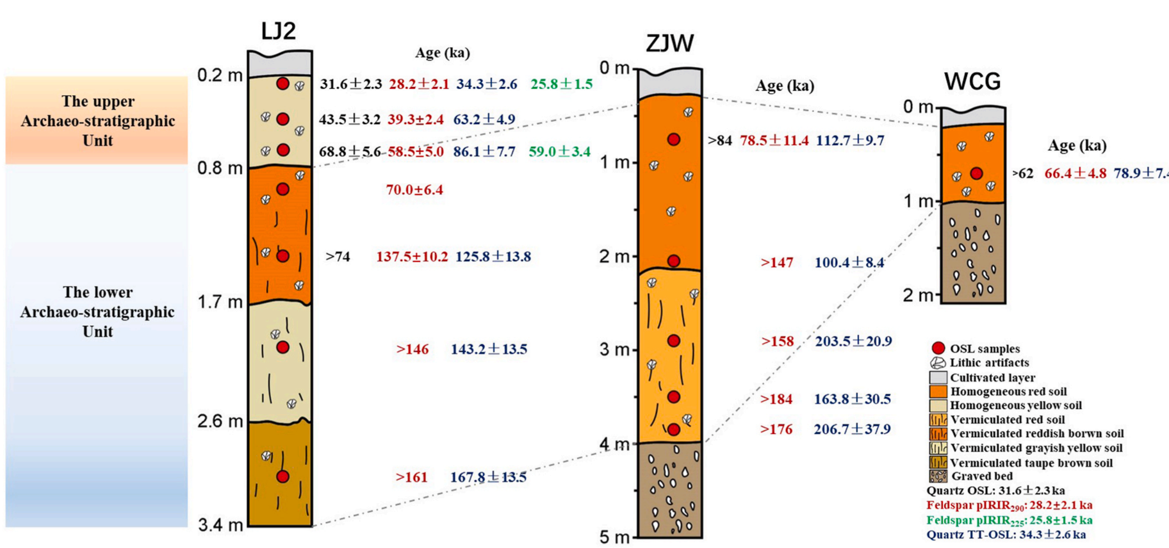

Fig. 7. Stratigraphy, luminescence ages and cultural phases of the study sites.

± 2.3 ka (120 ± 1 Gy) in the uppermost layer to >74 ka (>267 Gy) in the deepest layer. All samples from ZJW and WCG were saturated, yielding minimum ages of >84 ka and >62 ka, respectively. Quartz TT-OSL and K-feldspar pIRIR ($pIR_{50}IR_{225}$ and $pIR_{200}IR_{290}$) produced consistent age estimates between ~30 ka and ~130 ka for depths of 25–145 cm at LJ2.

The $pIR_{200}IR_{290}$ signal often approached saturation, producing minimum ages of >161 ka, while quartz TT-OSL yielded an age of 168 ± 14 ka at the deepest level. At ZJW, quartz TT-OSL ages range from 113 ± 10 ka to 207 ± 38 ka. Most $pIR_{200}IR_{290}$ results yielded minimum ages due to saturation, except for the uppermost sample at 79 ± 11 ka. At WCG,

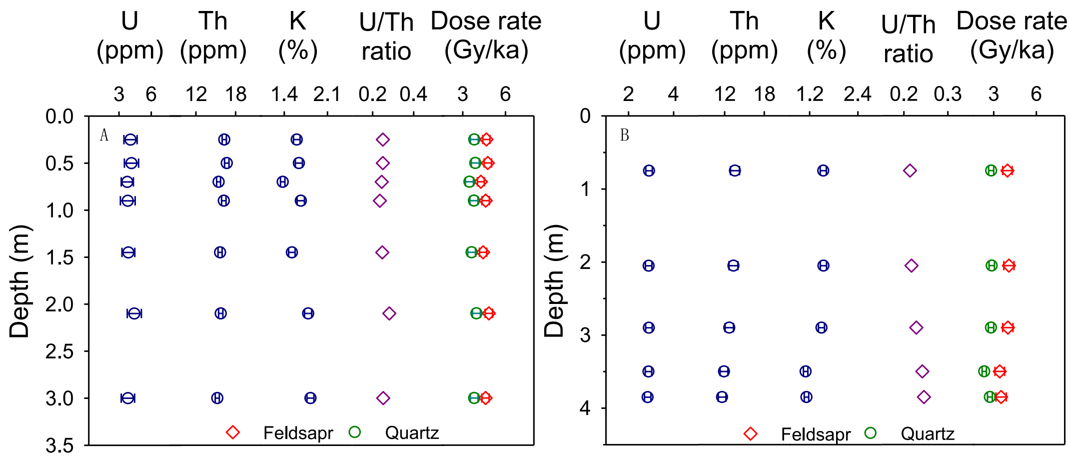

Fig. 8. Dosimetry summary for all samples from A) Liujia 2 (LJ2) and B) Zhangjiawan (ZJW) sites.

Table 1
Summary of sample code and depth, calculated dose rates, quartz OSL and K-feldspar pIRIR D_e values, and luminescence ages. (n) denotes the number of aliquots contributing to D_e. A) quartz SAR-OSL, B) quartz TT-OSL, C) K-feldspar $pIR_{200}IR_{290}$, and D) K-feldspar $pIR_{50}IR_{225}$.

Lab Number	Samples Number	Quartz OSL D_e (Gy)	Quartz TT-OSL D_e (Gy)	Feldspar $pIRIR_{290}$ D_e (Gy)	Feldspar $pIRIR_{225}$ D_e (Gy)	Aliquots (n) A/B/C/D	Quartz OSL Age (ka)	Quartz TT-OSL age (ka)	Feldspar $pIRIR_{290}$ age (ka)	Feldspar $pIRIR_{225}$ age (ka)
NJU3340	ZJW-70.5 cm	>268	361 ± 17	302 ± 41		6/5/8/0	>84	112.7 ± 9.7	78.5 ± 11.4	
NJU3341	ZJW-205 cm		330 ± 13	>583		0/6/3/0		100.4 ± 8.4	>147	
NJU3342	ZJW-290 cm		572 ± 42	>615		0/6/3/0		203.5 ± 20.9	>158	
NJU3343	ZJW-350 cm		382 ± 66	>612		0/6/4/0		163.8 ± 30.5	>184	
NJU3344	ZJW-385 cm		564 ± 97	>602		0/2/7/0		206.7 ± 37.9	>176	
NJU3650	WCG -70 cm	>186	236 ± 15	257 ± 13		13/5/5/0	>62	78.9 ± 7.4	66.4 ± 4.8	
NJU4005	LJ2-25 cm	120 ± 1	131 ± 3	132 ± 6	120 ± 3	13/6/6/6	31.6 ± 2.3	34.3 ± 2.6	28.2 ± 2.1	25.8 ± 1.5
NJU4075	LJ2-50 cm	169 ± 1	246 ± 6	187 ± 5		6/7/5/0	43.5 ± 3.2	63.2 ± 4.9	39.3 ± 2.4	
NJU4006	LJ2-70 cm	238 ± 7	299 ± 14	250 ± 16	252 ± 4	6/7/6/6	68.8 ± 5.6	86.1 ± 7.7	58.5 ± 5.0	59.0 ± 3.4
NJU4007	LJ2-90 cm			323 ± 24		0/0/4/0			70.0 ± 6.4	
NJU4073	LJ2-145 cm	>267	455 ± 37	609 ± 30		7/3/4/0	>74	125.8 ± 13.8	137.5 ± 10.2	
NJU4076	LJ2-210 cm		568 ± 35	>706		0/6/5/0		143.2 ± 13.5	>146	
NJU4074	LJ2-300 cm		637 ± 25	>739		0/6/7/0		167.8 ± 13.5	>161	

quartz TT-OSL and K-feldspar $pIR_{200}IR_{290}$ yielded consistent ages of 79 ± 7 ka and 66 ± 5 ka, respectively, falling within 1σ uncertainty.

4.2. Palaeoenvironment changes

The GSDs of the studied sediments exhibit a unimodal pattern (Fig. 9), consistent with typical aeolian loess from northern China and QRC in the middle to lower Yangtze River regions (Li et al., 1997, 2022; Xiong et al., 2002; Hu et al., 2005, 2015; Zhang et al., 2019). This pattern supports a predominantly aeolian origin, as observed at other Palaeolithic sites such as the Xuancheng section, where aeolian processes dominate except in the basal gravel layers (Fang et al., 1992; Zhao and Yang, 1995; Li et al., 1997; Hu et al., 2005). A secondary peak in the >100 μm fraction suggests localized input (Zhang et al., 2019; Lai et al., 2021b). Overall, the grain-size composition—characterized by low sand and high silt content—indicates consistent sedimentary homogenization throughout the profile (Fig. 9).

Mass-specific MS values range from 30 to 140 × 10^{-8} m^3/kg and define three stratigraphic zones (Fig. 10). Elevated MS values occur in the upper (0–0.6 m) and lower (1.8–3.4 m) layers, while the middle interval (0.6–1.8 m) exhibits significantly reduced values. This pattern resembles MS trends observed in the nearby Xiangyang section, Xuancheng, Anhui Province (Hu et al., 2003, 2009). Surface samples (0–0.6 m) show an average MS of 120 × 10^{-8} m^3/kg, decreasing to 56 × 10^{-8} m^3/kg in the middle zone, and increasing again to 78 × 10^{-8} m^3/kg in the lower zone.

Major elements SiO_2, Al_2O_3, and Fe_2O_3 collectively comprise over 80 % of the bulk geochemical composition (Table S4). CIA values range from 75.6 to 85.6, and WIP values range from 19.8 to 28.8, indicating sustained chemical weathering throughout the sequence (Nesbitt and Young, 1982; Fedo et al., 1995). These values are consistent with other QRC profiles in the middle and lower Yangtze River region (Deng et al., 2015), but are generally lower than those at Palaeolithic sites such as Huxushan (CIA: 84.5–85.9; Zhang et al., 2019) and Sandinggai (CIA:

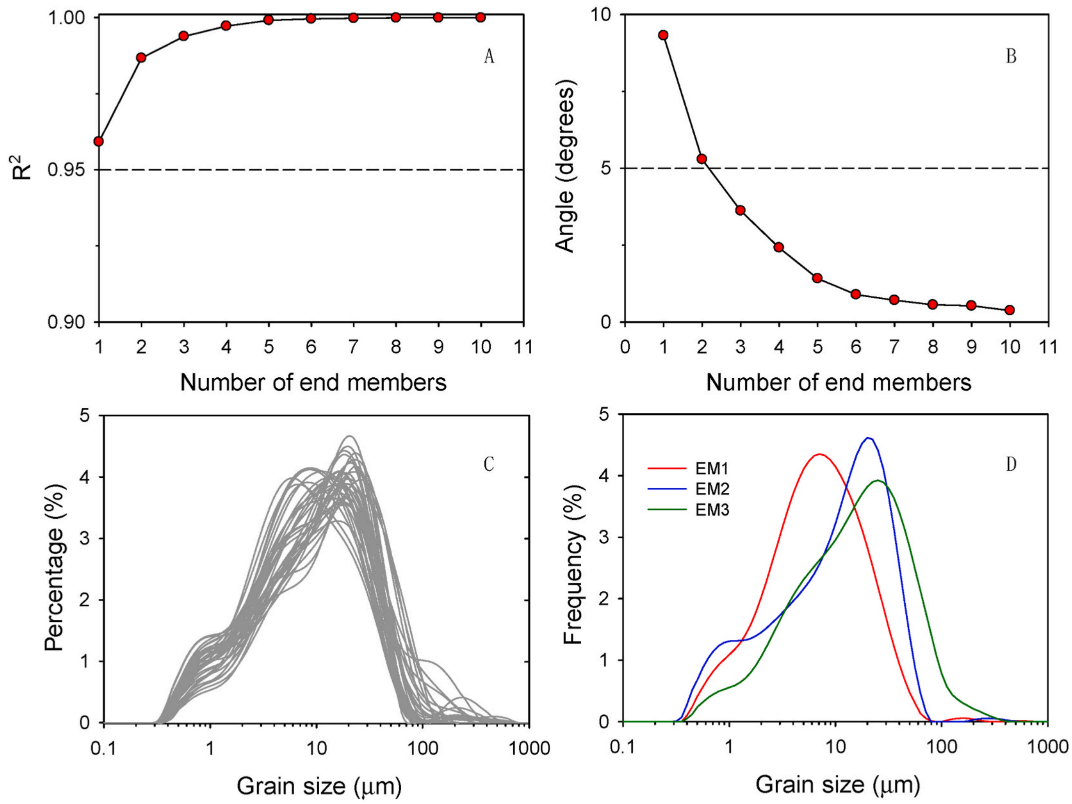

Fig. 9. Grain-size characteristics for the studied samples.

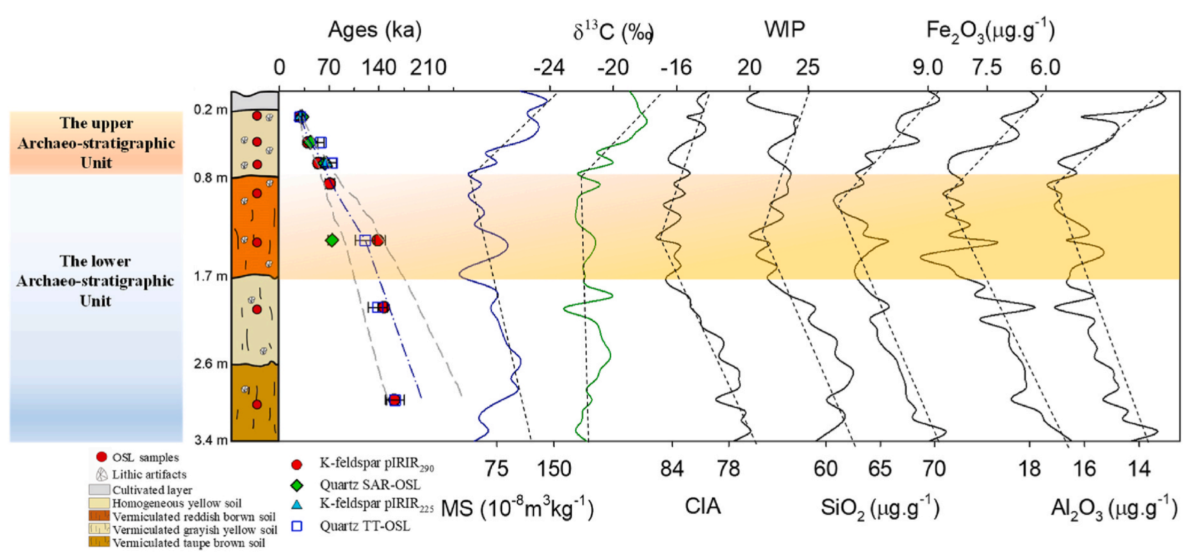

Fig. 10. Pedostratigraphy, luminescence chronology, archaeological horizons, and paleoenvironmental indices of the Liujia 2 (LJ2) site.

90.6–91.2; Li et al., 2022) in Hunan Province, suggesting moderately less intense weathering. CIA peaks between 0.6 and 1.8 m depth, whereas WIP shows an inverse trend, indicating temporal variability in weathering intensity.

Total organic carbon content remains generally below 1 %, likely due to intense weathering, limiting high-resolution interpretation of $\delta^{13}C_{org}$ values. Nevertheless, $\delta^{13}C_{org}$ shows a clear upward trend through the profile (Fig. 10). Below 0.6 m, values range from −23.03 ‰ to −20.04 ‰ (mean: −21.45 ‰); above 0.6 m, values shift to −19.34 ‰ to −17.87 ‰ (mean: −18.60 ‰). This trend is consistent with $\delta^{13}C_{org}$ patterns observed at the adjacent Xiangyang section in Xuancheng (Hu et al., 2003), and reflects a transition toward greater C_4 plant abundance, suggesting a shift from C_3 to C_4 vegetation dominance (O'Leary, 1988; Hu et al., 2003; Rao et al., 2008; Yang et al., 2014).

Integrated sedimentological and geochemical proxies reveal significant climatic fluctuations (Fig. 10). The low-MS zone (0.6–1.8 m) coincides with high CIA, low WIP, and evidence of gleying, indicating a warm and humid phase that enhanced chemical weathering and magnetic mineral dissolution (Lü et al., 1994; Yang et al., 1995; Hu et al., 2009). This interval also shows decreased SiO_2 and increased Al_2O_3 and Fe_2O_3, consistent with intensified pedogenesis. The $\delta^{13}C_{org}$ trend in the upper profile suggests increasing aridity associated with C_4 vegetation expansion. Collectively, these findings indicate a transition from a humid to a drier climate regime, consistent with regional records of Asian summer monsoon (ASM) variability (Huang et al., 2001; Rao et al., 2012; Jiang et al., 2019).

5. Discussion

5.1. Chronological framework of the Palaeolithic sites

The luminescence ages, supported by radionuclide concentrations, dose rates, and D_e values (Table 1 and S3), define a consistent and stratigraphically coherent chronological framework for the investigated Palaeolithic sites (Figs. 7 and 10). At the LJ2 site, quartz SAR-OSL ages are broadly consistent with K-feldspar $pIR_{200}IR_{290}$ and $pIR_{50}IR_{225}$ results within the upper 70 cm, covering the past ~70 ka during which the quartz OSL signal remains below saturation (Fig. 7). A gleyed paleosol layer identified between 0.9 and 1.45 m, dated to 70 ± 6 to 138 ± 10 ka (Figs. 7 and 10), corresponds to the transition from the Last Interglacial (MIS 5) to the early Last Glacial period (MIS 4), thereby providing independent support for the established chronological model. Our chronological framework is further corroborated by OSL-dated QRC sequences from northern Xuancheng, Anhui Province, where Last Glacial loess-like deposits overlie Last Interglacial reticulated red clay (Hu et al., 2015).

Despite this general agreement, quartz TT-OSL ages are consistently older than those derived from SAR-OSL and K-feldspar pIRIR protocols (Fig. 7). This offset is likely attributable to the slower bleaching kinetics of the TT-OSL signal, particularly given the significant residual dose (~19 ± 1 Gy) that was subtracted prior to final D_e determination. This interpretation is strongly supported by solar simulator bleaching experiments (Fig. 6A) and is consistent with previous findings (Wang et al., 2006b; Tsukamoto et al., 2008; Yi et al., 2012; Liu et al., 2016). Notably, despite a lack of signal saturation in deeper samples from LJ2 and ZJW, TT-OSL ages do not show proportional increases with depth, reflecting complex signal behavior that influences age estimates. In contrast, the stratigraphic consistency of U and Th concentrations and stable major element compositions (Fig. 8; Table S4) indicate a geochemically homogeneous sedimentary environment. Moderately elevated U/Th ratios, combined with lower CIA and higher WIP values relative to lateritic deposits at other Palaeolithic sites in Hunan and Fujian, suggest less intense chemical weathering (Zhang et al., 2019; Jin et al., 2021, 2023; Li et al., 2022). These factors imply minimal diagenetic alteration of dose rate conditions, enhancing the reliability of K-feldspar $pIR_{200}IR_{290}$ ages for deposits older than 70 ka. While quartz TT-OSL may overestimate burial ages due to incomplete bleaching, its extended saturation threshold provides useful maximum age constraints. Consequently, an integrated chronological model was developed, primarily grounded in well-validated quartz SAR-OSL and K-feldspar pIRIR ages, and supplemented with TT-OSL data to build a robust temporal framework for the sedimentary sequences (Fig. 10).

This chronology places the sediment accumulation between ~200 and 30 ka, corresponding to the late Middle and Late Pleistocene (Table 1; Fig. 7). These dates are consistent with those from multiple sites in the middle Yangtze Valley (Fig. 11), including Sandinggai, Fengshuzui, and Huxushan in Hunan Province, central southern China (Lai et al., 2021a; Zhang et al., 2019; Li et al., 2022). At LJ2, two major occupational phases are clearly distinguishable (Fig. 7): the lower AU (vermiculated paleosol, ~200–70 ka; MIS 5–7), associated with a small number of LCTs, and the upper AU (homogeneous yellow loam, ~60–30 ka; MIS 3), characterized by numerous small flakes and flaked tools (Fig. 3).

Since the initial discovery of Palaeolithic sites in the Shuiyangjiang River Basin in 1987, significant archaeological findings at locations such as Chenshan and Macun in Xuancheng (Fang, 1988, 1997; Dong and Zhan, 2020; Dong, 2025b), as well as Anyouzhuang, Guanshan, and Maozhushan in Ningguo (Fang et al., 2001; Dong and Zhan, 2023,

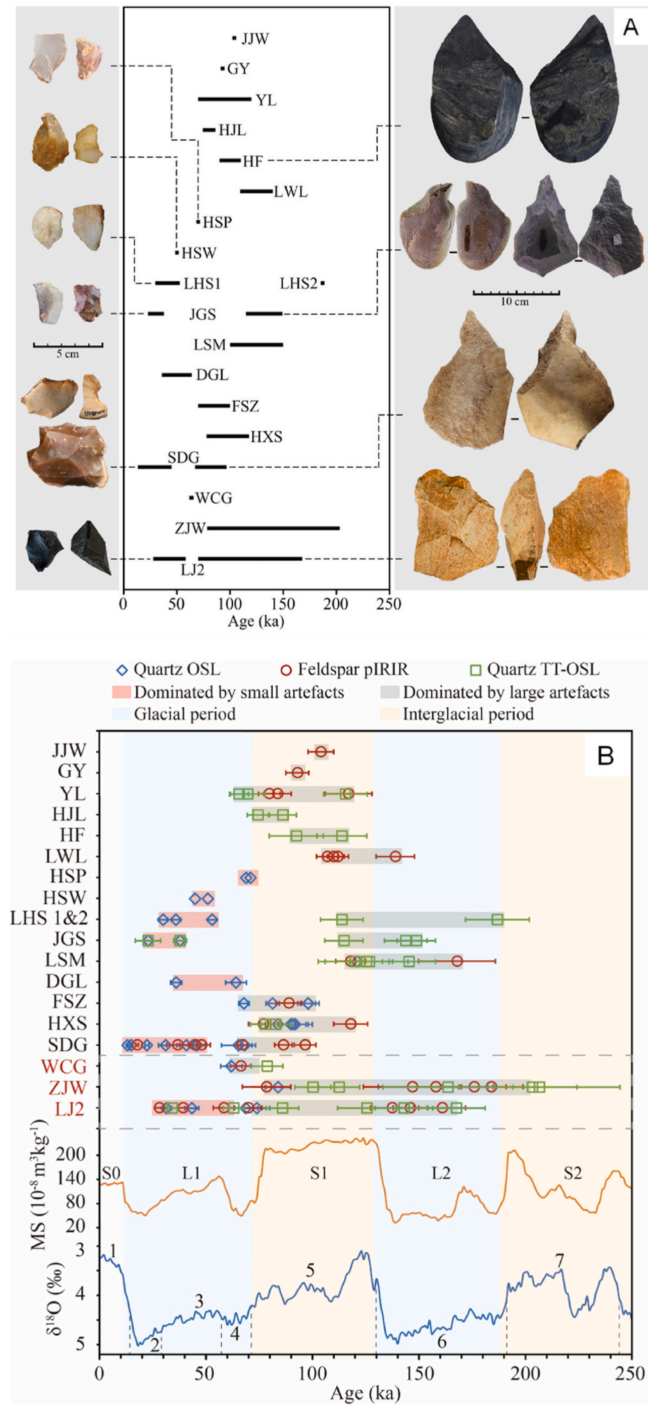

Fig. 11. Chronostratigraphic correlation of lithic technologies: A) Typological transitions and B) Regional comparisons. Sites analyzed in this study include ZJW (Zhangjiawan), WCG (Wangchenggang), and LJ2 (Liujia 2). Additional comparative sites encompass JJW (Jijiawan; Wang et al., 2014a Zhuo et al., 2016), GY (Ganyu; Wang et al., 2014a; Zhuo et al., 2016), YL (Yanling; Li et al., 2023), HJL (Hejialiang; Sun et al., 2012; Wang et al., 2014b), HF (Houfang; Li et al., 2018a,2018b), LWL (Longwanling; Guo et al., 2025), HSP (Houshanpo; Guo et al., 2021), HSW (Huoshiwa; Guo et al., 2021), LHS1 & LHS2 (Luohansi 1 and Luohansi 2; Yan et al., 2024), JGS (Jigongshan; Guo et al., 2020), LSM (Lanshanmiao; Lu et al., 2020), DGL (Daguling; Fang et al., 2003), FSZ (Fengshuzui; Zhang et al., 2019), HXS (Huxushan; Lai et al., 2021a), and SDG (Sandinggai; Li et al., 2022), all located within the Qinling Mountain region and the middle to lower reaches of the Yangtze River.

2025), have established this region as a key area for early human occupation. Hominin fossils recovered from nearby cave sites—including Hexian, Chaoxian, Nanjing, and Hualongdong—have been dated to approximately 0.6–0.1 Ma using U-series and electron spin resonance (ESR) techniques, indicating a concentration of Middle Pleistocene human remains in the region (Grün et al., 1998; Zhao et al., 2001; Shen et al., 2010; Wu et al., 2019). Similarly, QRC deposits in Xuancheng have been assigned ages ranging from ~1.00 to 0.10 Ma based on stratigraphic correlations and ESR dating (Zhao and Yang, 1995; Yang et al., 1996). Despite these findings, only a limited number of open-air Palaeolithic sites in the middle–lower Yangtze River region have been directly dated using luminescence methods (Figs. 1 and 11). These include Lanshanmiao (LSM, ~150–100 ka; Lu et al., 2020), Daguling (DGL, ~64.2–36.1 ka; Fang et al., 2003), Houshanpo (HSP, >70 ka; Guo et al., 2021), Huoshiwa (HSW, >50 ka; Guo et al., 2021), Luohansi 1 (LHS1, 53–30 ka; Yan et al., 2024), Luohansi 2 (LHS2, ~187 ka; Yan et al., 2024), Jigongshan (JGS, ~38–23 ka for the upper cultural layer and ~149–115 ka for the lower cultural layer; Guo et al., 2020), Fengshuzui (FSZ, ~100–70 ka; Zhang et al., 2019), Huxushan (HXS, ~118–78 ka; Lai et al., 2021a), and Sandinggai (SDG, ~96.6–13.3 ka; Li et al., 2022). The availability of well-dated Late Pleistocene assemblages, together with typological similarities among Middle Pleistocene artifacts, provides important evidence for understanding *Homo sapiens* dispersal and lithic technological transitions in central southern China.

In this context, the three Palaeolithic sites examined in this study—particularly the younger occupation layers at LJ2—help address a critical chronological gap in the Late Pleistocene archaeological record of Anhui Province, offering valuable insights into regional prehistoric developments in southern China.

5.2. Lithic technological transitions in CLR

In South China, stone artifact assemblages, including those from the lower Yangtze River region, have been variably classified as part of the Pebble Tool Industry (Zhang, 1999), simple core and flake techno-complexes (Bar-Yosef and Wang, 2012; Gao, 2013), Mode 1 (Oldowan) technology (Pei, 2014; Guan et al., 2018), or the Pick-Chopper Industry (Gao and Guan, 2016). However, artifact assemblages from the three Palaeolithic sites in the CLR are distinguished by large flakes detached from giant or large cores, which were subsequently shaped into Acheulean large tools, such as handaxes, knives, and massive scrapers (Zhan et al., 2022, 2025; Dong, 2025a). A stratigraphically significant technological shift is evident at the LJ2 site. The lower AU, associated with vermiculated soil (~200–70 ka), contains 353 larger lithic specimens, with an average length of 45.8 mm and 20 pieces exceeding 100 mm. These artifacts, predominantly made of quartzite (56.6 %) and quartz sandstone (30.0 %), form an assemblage marked by heavy-duty tools, such as knives, cleavers, and massive scrapers, which were mostly made from large flakes (Fig. 3; Table S1). This toolkit is fundamentally different from simple core-flake technologies and may represent a local Acheulean-like technological complex (Semaw et al., 2009; Zhan et al., 2022, 2025; Dong, 2025a), aligning with contemporaneous and earlier industries found in the Qinling Mountain Range (QMR) and the middle-lower Yangtze Valley (Fig. 11A), such as those at Jijiawan (JJW, ~104 ka; Wang et al., 2014a; Zhuo et al., 2016), Yanling (YL, 120–70 ka; Li et al., 2023), Hejialiang (LJL, 86–75 ka; Sun et al., 2012; Wang et al., 2014b), Houfang (HF, 110–90 ka; Li et al., 2018a,b), Longwanling (LWL, ~140–110 ka; Guo et al., 2025), Luohansi 2 (LHS2, ~187 ka; Yan et al., 2024), the lower culture layer of Jigongshan (JGS, ~149–115 ka; Guo et al., 2020), Fengshuzui (FSZ, ~100–70 ka; Zhang et al., 2019), Huxushan (HXS, ~118–78 ka; Lai et al., 2021a), and the lower culture layer of Sandinggai (SDG, ~96.6–70 ka; Li et al., 2022).

In stark contrast, the upper AU (homogeneous yellow soil, ~60–30 ka) contains 771 artifacts, characterized primarily by light-duty implements, with a mean length of 25–26 mm. This assemblage consists mostly of small flakes and retouched tools, such as scrapers and denticulates, predominantly made of black rhyolitic tuff (49.3 %), supplemented by quartz (22.4 %), quartzite (22.2 %), and quartz sandstone (5.8 %) (Table S1). The distinct raw material preferences and the dramatic reduction in artifact dimensions between the upper and lower cultural layers reflect a clear technological transition—from the large flake-based Acheulean tradition to the systematic production of small flakes (Fig. 3), in line with the concept of lithic miniaturization (Shipton, 2023). A comparable technological progression is evident at other regional sites. For example, at Sandinggai (SDG) and Jigongshan (JGS), LCT-dominated assemblages in lower layers are replaced by small flake tools in the upper layers (Liu and Wang, 2001; Guo et al., 2020; Li et al., 2022). Widespread evidence from the middle-lower Yangtze region further supports this trend, with miniaturized flake tool industries documented at multiple sites, such as Daguling (DGL, ~64.2–36.1 ka; Li et al., 1994; Fang et al., 2003), Shanghu (SH, ~26 ka; Zhao et al., 2023), Houshanpo (HSP, >70 ka; Guo et al., 2021), Huoshiwa (HSW, >50 ka; Guo et al., 2021), and Luohansi 1 (LHS1, ~53–30 ka; Yan et al., 2024), spanning approximately 70–13 ka (Fig. 11A).

In summary, the lithic assemblages from the CLR illustrate significant technological changes during the Late Pleistocene, marked by a dramatic reduction in tool size, selective use of high-quality raw materials, and a predominant focus on small flake tools. These transitions collectively highlight a key shift in hominin technological behavior within the region.

5.3. Influence of palaeoclimate on technological strategies and human occupation

The decline of LCTs has often been linked to the emergence of new technological systems (Adler et al., 2014; Richter et al., 2017; Moncel et al., 2018). Recent hypotheses increasingly suggest that fluctuating hydroclimatic conditions and heightened climate variability during the Late Pleistocene reshaped ecosystems and resource availability (DeMenocal, 2011; Potts et al., 2018, 2020; Lupien et al., 2020, 2022), driving hominin adaptations through either migration or technological innovation (Yang et al., 2020, 2024). In southern China, the appearance of small flake tools during the Late Palaeolithic (~50–10 ka) has been associated with potential human dispersals from the north, with forager populations adapting these tools to local ecological conditions (Wang, 2017; Xie et al., 2020).

Our study area is located within the monsoon-influenced core region, where the ASM brings distinct seasonal precipitation (Lu et al., 2011, 2017; Deng et al., 2015). Multi-proxy records from the LJ2 profile, integrating MS, $\delta^{13}C_{org}$, and geochemical data, reveal a crucial transition from persistent warm-humid conditions in the lower AU to drier, cooler climates in the upper AU (Fig. 10). This shift marks a significant environmental reorganization, including a change from C_3-dominated plant communities to mixed C_3/C_4 communities. This regional climatic trend is supported by multiple independent archives: granulometric and geochemical records from the Xuancheng QRC sequence document a marked shift from Last Interglacial to Last Glacial conditions, characterized by the cessation of rubification and the onset of loess deposition around ~60 ka (Hu et al., 2015). Concurrently, high-resolution pollen data from Chaohu Lake indicate the establishment of open forest-steppe vegetation under relatively cold-arid conditions during the Last Deglaciation (Han et al., 2024). Additional support comes from palaeoenvironmental records at Gucheng Lake (Yang and Wang, 1996) and the Nanjing-Jiangyin stratigraphic sequence (Xu and Zhu, 1984; Xu et al., 1987).

Against this climatic backdrop, we propose that the observed lithic technological shifts in the CLR reflect behavioral adjustments to evolving environmental pressures. The trend toward lithic miniaturization, characterized by small flakes and extensively retouched tools, likely represents an adaptive strategy in response to cooler, drier conditions and the resulting patchy resource distribution. The concentration of small flake tools in the upper AU at LJ2 during MIS 3 reflects localized technological innovation driven by climate-induced environmental stress (Yang et al., 2024). While climatic variability in the Yangtze Valley was less extreme compared to northern China, the glacial-interglacial shifts nonetheless had a significant influence on technological trajectories (Lu et al., 2011, 2017; Pei et al., 2013; Huang et al., 2017), acting as a key stimulus for lithic reorganization during the Last Interglacial-Glacial transition (Fig. 11B).

These technological adaptations unfolded alongside sustained hominin occupation of the region. Spatiotemporal analyses indicate an intensified human presence in the QMR and lower Yangtze Valley during the late Middle Pleistocene (Qin and Sun, 2023), empirically validating monsoonal China as an ecologically favorable habitat for early human populations (Lu et al., 2017). The abundance of stone artifacts across the studied CLR sites attests to recurrent hominin activity since the late Middle Pleistocene (Dong, 2025a; Zhan et al., 2025). This continuous occupation is supported by the region's moderate climate, accessible freshwater resources, and forest-grassland mosaic ecosystems, which together provided a stable foundation for human subsistence and technological experimentation (Bae et al., 2018; Dennell et al., 2020).

6. Conclusions

This study establishes a robust luminescence-based chronology for three Palaeolithic sites in the CLR, Anhui Province, South China, employing a multi-method approach that includes quartz SAR-OSL, TT-OSL, and K-feldspar pIRIR ($pIR_{50}IR_{225}$ and $pIR_{200}IR_{290}$) dating. These sites have yielded a rich assemblage of stone artifacts, including typologically verified LCTs, such as handaxes.

The ages derived from quartz SAR-OSL and K-feldspar pIRIR are in strong agreement, reinforcing the reliability of the chronological framework. In contrast, quartz TT-OSL consistently produced overestimated ages, highlighting the need for caution in applying this method in similar contexts.

The integrated chronology reveals that hominin occupation persisted from approximately 200 to 30 ka, spanning the late Middle to Late Pleistocene and filling a significant gap in the regional archaeological record. Specifically, the lower AU at the LJ2 site, containing knives and handaxes, dates to 200–70 ka, representing a LCT-bearing technocomplex during MIS 5–7. In contrast, the overlying deposits, dated to 60–30 ka, are rich in small flakes and flaked tools, marking the emergence and development of a local small flake-based reduction system. These technological shifts reflect human adaptation to climatic changes from the Last Interglaciation to the Last Glaciation. Overall, our findings underscore the importance of the CLR as a key area for understanding behavioural adaptations to glacial–interglacial cycles in southern China.

Credit author statement

Shuangwen Yi: Conceptualization, Data curation, Methodology, Software, Visualization, Writing – original draft. **Zhe Dong:** Conceptualization, Data curation, Writing – original draft. **Shijia Zhan:** Data curation, Validation, Writing – review & editing. **Shuwen Pei:** Validation, Writing – review & editing. **Huayu Lu:** Funding acquisition, Resources, Writing – review & editing.

Declaration of competing interest

The authors declare that they have no known competing financial interests or personal relationships that could have appeared to influence the work reported in this paper.

Acknowledgements

We sincerely thank Mr. Jiang Wu, Mr. Zaizhong Wen, and Mr. Chuanbin Yang for their invaluable assistance during field investigations and laboratory analyses. We are especially grateful to Ms. Xiaoqi Guo for her significant contributions to the graphical presentations. This research was supported by the National Natural Science Foundation of China (Grant No. 42361144846), the National Key R&D Program of China (2023YFF0804703), and the Archaeological Talent Promotion Program of China (Program No. 2024-278).

Appendix A. Supplementary data

Supplementary data to this article can be found online at https://doi.org/10.1016/j.quascirev.2025.109728.

Data availability

All data and/or code is contained within the submission.

References

Adamiec, G., Duller, G.A.T., Roberts, H.M., Wintle, A.G., 2010. Improving the TT-OSL SAR protocol through source trap characterization. Radiat. Meas. 45, 768–777.
Adler, D.S., Wilkinson, K.N., Blockley, S., Mark, D.E., Pinhasi, R., Schmidt-Magee, B.A., et al., 2014. Early Levallois technology and the lower to middle paleolithic transition in the southern caucasus. Science 345, 1609–1613.
Aitken, M.J., 1985. Thermoluminescence Dating. Academic Press, London.
Auclair, M., Lamothe, M., Huot, S., 2003. Measurement of anomalous fading for feldspar IRSL using SAR. Radiat. Meas. 37, 487–492.
Bae, C.J., Douka, K., Petraglia, M.D., 2017. On the origin of modern humans: asian perspectives. Science 358 eaai9067.
Bae, C.J., 2017. Late pleistocene human evolution in eastern Asia: behavioral perspectives. Curr. Anthropol. 58, 514–526.
Bae, C.J., 2024. The Paleoanthropology of Eastern Asia. University of Hawai'i Press, Honolulu.
Bae, C.J., Li, F., Cheng, L.L., Wang, W., Hong, H.L., 2018. Hominin distribution and density patterns in pleistocene China: climatic influences. Palaeogeogr. Palaeoclimatol. Palaeoecol. 512, 118–131.
Bae, C.J., Wang, W., Zhao, J.X., Huang, S.M., Tian, F., Shen, G.J., 2014. Modern human teeth from late Pleistocene Luna Cave (Guangxi, China). Quat. Int. 354, 169–183.
Bar-Yosef, O., Wang, Y.P., 2012. Paleolithic archaeology in China. Annu. Rev. Anthropol. 41, 319–335.
Buylaert, J.P., Murray, A.S., Thomsen, K.J., Jain, M., 2009. Testing the potential of an elevated temperature IRSL signal from K-feldspar. Radiat. Meas. 44, 560–565.
Buylaert, J.P., Jain, M., Murray, A.S., Thomsen, K.J., Thiel, C., Sohbati, R., 2012. A robust feldspar luminescence dating method for middle and Late Pleistocene sediments. Boreas 41, 435–451.
Colarossi, D., Duller, G.A.T., Roberts, H.M., Tooth, S., Lyons, J.R., 2015. Comparison of paired quartz OSL and feldspar post-IR IRSL dose distributions in poorly bleached fluvial sediments from South Africa. Quat. Geochronol. 30 (B), 233–238.
Cunningham, A.C., Wallinga, J., 2010. Selection of integration time intervals for quartz OSL decay curves. Quat. Geochronol. 5, 657–666.
DeMenocal, P.B., 2011. Climate and human evolution. Science 331, 540–542.
Deng, H.Y., Zheng, X.M., Yang, L.H., Ren, S.F., Liu, F., 2015. Magnetic properties of Quaternary red earth profile in Yangtze River Valley and its paleoenvironmental implications. Acta Sedimentol. Sin. 33, 285–298 (in Chinese with English abstract).
Dennell, R., Martinón-Torres, M., de Castro, J.M.B., Gao, X., 2020. A demographic history of Late Pleistocene China. Quat. Int. 559, 4–13.
Dong, Z., Zhan, S.J., 2020. A preliminary report on the survey and excavation at Macun Paleolithic Site in Xuancheng, Anhui Province. Acta Anthropol. Sin. 39 (1), 74–85 (in Chinese with English abstract).
Dong, Z., 2025a. A preliminary report on the excavation at the CHLJ2 site, Anhui Province. Archaeology 6, 3–17 (in Chinese with English abstract).
Dong, Z., 2025b. Study of Ancient human lithic technology at the chenshan site in the Shuiyang River Basin, Anhui. South. Cult. 305 (3), 80–89 (in Chinese with English abstract).
Dong, Z., Pei, S.W., Yuan, S.F., 2019. A preliminary report on the Paleolithic survey in Shuiyangjiang River system, Anhui Province in 2017. Acta Anthropol. Sin. 38 (2), 223–231 (in Chinese with English abstract).
Dong, Z., Zhan, S.J., 2023. Stone artifacts newly discovered from the Paleolithic Archaeological Survey in the area along the Yangtze River in Anhui. South. Cult. 3, 100–107 (in Chinese with English abstract).
Dong, Z., Zhan, S.J., 2022. A preliminary report on the survey and excavation at Anyouzhuang Paleolithic site in Ningguo City, Anhui Province. Acta Anthropol. Sin. 41 (2), 342–353 (in Chinese with English abstract).
Dong, Z., Zhan, S.J., 2025. Lithic technology of ancient hominins of the Guanshan site in Shuiyangjiang River Basin, Anhui Province. Acta Anthropol. Sin. 44 (e). https://doi.org/10.16359/j.1000-3193/AAS.2025.0086 (in Chinese with English abstract).
Duller, G.A.T., 2003. Distinguishing quartz and feldspar in single grain luminescence measurements. Radiat. Meas. 37, 161–165.
Fang, D.S., 1990. Discovery and study of paleolithic in Wangchenggang, Chaohu City. Heritage Studies 6, 19–35 (in Chinese).
Fang, D.S., Han, L.G., 1993. The excavation report of Wangchenggang Paleolithic site in Chaohu City. Cultural Relics Research 8, 80–92 (in Chinese with English abstract).

Fang, Y.S., 1988. A preliminary report on the Paleolithic survey of the Shuiyangjiang Paleolithic site-complex, Anhui Province. Heritage Studies 3, 74–83 (in Chinese).
Fang, Y.S., 1997. A report on excavation of Chenshan locality in 1988, Anhui Province. Acta Anthropol. Sin. 16 (2), 96–106 (in Chinese with English abstract).
Fang, Y.S., 2002. A report on the Paleolithic survey of Southern Jiangsu. Sooutheast Culture 1, 17–25 (in Chinese with English abstract).
Fang, Y.S., Huang, Y.P., Liang, R.Y., Chen, Y., Peng, D.Q., 2001. Discovery of early paleolithic relic at Maozhushan site in Ningguo, Anhui Province. Acta Anthropol. Sin. 20 (2), 115–124 (in Chinese with English abstract).
Fang, Y.S., Li, X.S., Yang, D.Y., 2003. Paleoenvironmental and chronological analyses of the Daguling paleolithic locality, Xinyu city, Jiangxi Province. Acta Anthropol. Sin. 22 (2), 139–144 (in Chinese with English abstract).
Fang, Y.S., Yang, D.Y., Han, H.Y., Zhou, L.F., 1992. Taphonomy study of Paleolithic site group of Shuiyang river. Acta Anthropol. Sin. 2, 134–142.
Fedo, C.M., Nesbitt, H.W., Young, G.M., 1995. Unraveling the effects of potassium metasomatism in sedimentary-rocks and paleosols, with implications for paleoweathering conditions and provenance. Geology 23, 921–924.
Fu, Q.M., Meyer, M., Gao, X., Stenzel, U., Burbano, H.A., Kelso, J., Pääbo, S., 2013. DNA analysis of an early modern human from Tianyuan Cave, China. Proc. Natl. Acad. Sci. U.S.A. 110 (6), 2223–2227.
Gao, X., 2013. Paleolithic cultures in China: uniqueness and divergence. Curr. Anthropol. 54, S358–S370.
Gao, X., Guan, Y., 2016. Handaxes and the pick-chopper industry of Pleistocene China. Quat. Int. S1040618216302336.
Gao, X., Peng, F., Fu, Q.M., Li, F., 2017. New progress in understanding the origins of modern humans in China. Sci. China Earth Sci. 60, 2160–2170.
Ge, J.Y., Xing, S., Grün, R., Deng, C.L., Jiang, Y.J., Jiang, T.Y., Yang, S.X., Zhao, K.L., Gao, X., Yang, H.L., Guo, Z.T., Petraglia, M.D., Shao, Q.F., 2024. New Late Pleistocene age for the Homo sapiens skeleton from Liujiang southern China. Nat. Commun. 15 (2024), 3611.
Grün, R., Huang, P.H., Huang, W.P., McDermott, F., Thorne, A., Stringer, C.B., Yan, G., 1998. ESR and U-series analyses of teeth from the palaeoanthropological site of Hexian, Anhui Province, China. J. Hum. Evol. 34, 555–564.
Guan, Y., Xu, X.M., Kuman, K., Wu, H.Z., Zhou, Z.Y., Gao, X., 2018. The absence of Acheulean: qiliting Mode 1 site and the Mode 1 occupations in southeast China. Quat. Int. 480, 152–165.
Guérin, G., Mercier, N., Adamiec, C., 2011. Dose-rate conversion factors: update. Ancient TL 29, 5–8.
Guo, X.Q., Lu, C.Q., Qin, Z.Y., Dong, B., Yu, L.P., Bae, C.J., Sun, X.F., 2025. Single-grain K-feldspar pIRIR dating of the Longwanling handaxe-bearing site in the Hanjiang river valley, central China. Quat. Sci. Rev., 109194
Guo, X.Q., Lu, C.Q., Sun, X.F., Liu, D.K., Lu, Y., 2021. Luminescence dating of the Huoshiwa and Houshanpo Paleolithic sites in Hanjiang River Valley, Central China. Quat. Int. 586, 133–144.
Guo, X.Q., Sun, X.F., Feng, X.B., Yi, S.W., Zhou, X.Y., Liu, D.Y., Tang, Q.Q., 2020. Luminescence dating of the Jigongshan Paleolithic site in Hubei Province, southern China. Quat. Int. 554, 36–44.
Han, X.Y., Shu, J.W., Wu, L., Li, B.H., Lu, S.G., Chen, W., Ge, J.L., 2024. Transformation of regional vegetation driven by climate change during the last deglacial-early Holocene at Chaohu Lake, eastern China: new pollen insights. Rev. Palaeobot. Palynol. 326, 105115.
Hu, X.F., Cheng, T.F., Wu, H.X., 2003. Do multiple cycles of aeolian deposit-pedogenesis exist in the reticulate red clay sections in southern China? Chin. Sci. Bull. 48, 1251–1258.
Hu, X.F., Du, Y., Liu, X.J., Zhang, G.L., Jiang, Y., Xue, Y., 2015. Polypedogenic case of loess overlyingred clay as a response to the last Glacial-Interglacial cycle in midsubtropical Southeast China. Aeolian Res. 16, 125–142.
Hu, X.F., Wei, J., Xu, L.F., Zhang, G.L., Zhang, W.G., 2009. Magnetic susceptibility of the Quaternary Red Clay in subtropical China and its paleoenvironmental implications. Palaeogeogr. Palaeoclimatol. Palaeoecol. 279 (3–4), 216–232.
Hu, X.F., Yu, Z., Shen, M.N., 2005. Grain-size evidence for multiple origins of the reticulate red clay in southern China. Chin. Sci. Bull. 50, 910–918.
Huang, S.M., Hong, H.L., Bae, C.J., Cheng, L.L., Li, D.W., Liao, W., Yin, K., Wang, C.W., Wang, W., 2017. Paleoenvironmental background of the Early Pleistocene Gigantopithecus fauna in Bubing Basin, south China. Quat. Int. 434, 163–168.
Huang, W.B., Fang, D.S., Ye, Y.X., 1982. Preliminary study on the fossil hominid skull and fauna of Hexian, Anhui. Vertebr. Palasiat. 20 (3), 248–256 (in Chinese with English abstract).
Huang, W.P., Fang, D.S., Ye, Y.X., 1981. Observations on the *Homo erectus* skull that was found from Longtandong, Hexian, Anhui. Chin. Sci. Bull. 26, 1508–1510 (in Chinese).
Huang, Y.S., Street-Perrott, F.A., Metcalfe, S.E., Brenner, M., Moreland, M., Freeman, K. H., 2001. Climate change as the dominant control on glacial-interglacial variations in C3 and C4 plant abundance. Science 293, 1647–1651.
Hublin, J.J., 2021. How old are the oldest *Homo sapiens* in Far East Asia? Proc. Natl. Acad. Sci. U.S.A. 118, e2101173118.
Huntley, D.J., Baril, M.R., 1997. The K content of the K-feldspars being measured in optical dating or in thermoluminescence dating. Ancient TL 15, 11–13.
Huntley, D.J., Hancock, R.G.V., 2001. The Rb contents of the K-feldspar grains being measured in optical dating. Ancient TL 19, 43–46.
Huntley, D.J., Lamothe, M., 2001. Ubiquity of anomalous fading in K-feldspars and the measurement and correction for it in optical dating. Can. J. Earth Sci. 38, 1093–1106.
Huntley, D.J., Lian, O.B., 2006. Some observations on tunnelling of trapped electrons in feldspars and their implications for optical dating. Quat. Sci. Rev. 25, 2503–2512.
Jacobs, Z., Li, B., Shunkov, M.V., Kozlikin, M.B., Bolikhovskaya, N.S., Agadjanian, A.K., Uliyanov, V.A., Vasiliev, S.K., O'Gorman, K., Derevianko, A.P., Roberts, R.G., 2019. Timing of archaic hominin occupation of Denisova Cave in southern Siberia. Nature 565, 594–599.
Jiang, W.Q., Wu, H.B., Li, Q., Lin, Y.T., Yu, Y.Y., 2019. Spatiotemporal changes in C_4 plant abundance in China since the last Glacial Maximum and their driving factors. Palaeogeogr. Palaeoclimatol. Palaeoecol. 518, 10–21.
Jin, J.H., Li, Z.Z., Cheng, Y., Xu, X., Li, Z.X., Liu, X.J., 2018. Late Pleistocene aeolian activity in Haitan Island, Southeast China: insights from optically stimulated luminescence dating of coastal dunes on marine terraces. J. Mt. Sci. 15 (8), 1777–1788.
Jin, J.H., Qiu, J.J., Ling, Z.Y., Wei, J.J., Zuo, X.X., Li, Z.Z., Hou, C.Y., Xu, D.Y., 2023. Luminescence chronology of reticulated laterites in the humid subtropical mountains of South China. Paleoceanogr. Paleoclimatol. 38 (11) e2022PA004603.
Jin, J.H., Wang, X.Y., Zhou, Z.Y., Huang, Y.M., Fan, X.C., Zuo, X.X., Li, Z.Z., Ling, Z.Y., Ren, Y.Q., Li, S.T., 2021. OSL chronology of a Palaeolithic site in a humid subtropical mountainous area of southeast China. J. Mt. Sci. 18 (8), 2012–2023.
Kars, R.H., Reimann, T., Ankjærgaard, C., Wallinga, J., 2014. Bleaching of the post-IR IRSL signal: new insights for feldspar luminescence dating. Boreas 37, 441–449.
Li, B., Jacobs, Z., Roberts, R.G., Li, S.H., 2014. Review and assessment of the potential of post-IR IRSL dating methods to circumvent the problem of anomalous fading in feldspar luminescence. Geochronometria 41, 178–201.
Li, B., Li, S.H., 2011. Luminescence dating of K-feldspar from sediments: a protocol without anomalous fading correction. Quat. Geochronol. 6, 468–479.
Li, B., Li, S.H., 2012. A reply to the comments by Thomsen et al. on "Luminescence dating of K-feldspar from sediments: a protocol without anomalous fading correction". Quat. Geochronol. 8, 49–51.
Li, C.R., Hou, Y.Z., Wang, Q., 1994. Material of Paleolithic from Xinyu, Jiangxi Province. Acta Anthropol. Sin. 13 (4), 309–313 (in Chinese with English abstract).
Li, H., Kuman, K., Li, C.R., 2018. What is currently (un)known about the Chinese Acheulean, with implications for hypotheses on the earlier dispersal of hominids. C. R. Palevol 17, 120–130.
Li, H., Li, Y.Y., Yu, L.P., Tu, H., Zhang, Y.Z., Sumner, A., Kuman, K., 2022. Continuous technological and behavioral development of late Pleistocene hominins in central South China: multidisciplinary analysis at Sandinggai. Quat. Sci. Rev. 298, 107850.
Li, H., Lotter, M.G., Kuman, K., Lei, L., Wang, W., 2021. Population dynamics during the Acheulean at ~0.8 Ma in east and Southeast Asia: considering the influence of two geological cataclysms. Palaeogeogr. Palaeoclimatol. Palaeoecol. 562, 109927.
Li, H., Wang, S.J., Lotter, M.G., Dennell, R., Kuman, K., Chen, F.H., 2024. The temporal-spatial evolution of handaxe technology in China: recent progress and future directions. Sci. Bull. 69, 2161–2165.
Li, J.M., Wang, S.J., Sun, X.F., Lu, H.Y., Zhang, X.B., Zhang, H.Y., Zhang, G.K., Xia, W.T., Bie, J.J., 2023. Excavation report of the Yanling paleolithic site in the Luonan Basin, Shaanxi Province. Acta Anthropol. Sin. 42 (e), 1–12 (in Chinese with English abstract).
Li, X.S., Yang, D.Y., Lu, H.Y., Han, H.Y., 1997. The grain-size features of Quaternary aeolian-dust deposition sequence in south Anhui and their significance. Mar. Geol. Quat. Geol. 4, 74-79+81-82.
Lai, H.C., Zhang, J.F., Li, Y.Y., Zhou, L.P., 2021b. Origin and provenance of Red Clay in north Hunan Province, China: Inferred from grain-size analysis and end-member modelling. Aeolian Res. 51,100714.
Li, Y.Y., 2020. Lithic Industries and Adaptation Behaviors: the Late Pleistocene Hominin Culture in the Lishui River Valley. Shanghai Chinese Classics Publishing House, Shanghai.
Li, Y.H., Zhou, Y.D., Sun, X.F., 2018b. The significance of the Age and Cha ne Opératoire in the lithic industry at Houfang Site, Yunxian County, Hubei Province. Jianghan Archaeology 2, 36–47 (in Chinese with English abstract).
Li, Y.H., Zhou, Y.D., Sun, X.F., Li, H., 2018a. New evidence of a lithic assemblage containing in situ Late Pleistocene bifaces from the Houfang site in the Hanshui River Valley, Central China. C. R. Palevol 17, 131–142.
Liu, D.Y., Wang, Y.P., 2001. A preliminary report on the excavation of Jigongshan site. Acta Anthropol. Sin. (2), 102–114. + 165-166 (in Chinese with English abstract).
Liu, J.F., Murray, A.S., Buylaert, J.P., Jain, M., Chen, J., Lu, Y.C., 2016. Stability of fine-grained TT-OSL and post-IR IRSL signals from a c. 1 Ma sequence of aeolian and lacustrine deposits from the Nihewan Basin (northern China). Boreas 45, 703–714.
Liu, W., Martinon-Torres, M., Cai, Y.J., Xing, S., Tong, H.W., Pei, S.W., Sier, M.J., Wu, X. H., Edwards, R.L., Cheng, H., Li, Y.Y., Yang, X.X., Bermúdez de Castro, J.M., Wu, X. J., 2015. The earliest unequivocally modern humans in southern China. Nature 526, 696–699.
Liu, W., Wu, X.Z., Pei, S.W., Wu, X.J., Norton, C.J., 2010. Huanglong Cave: a late Pleistocene human fossil site in Hubei Province, China. Quat. Int. 211, 29–41.
Lowick, S.E., Trauerstein, M., Preusser, F., 2012. Testing the application of post IR-IRSL dating to fine grain waterlain sediments. Quat. Geochronol. 8, 33–40.
Lu, H.Y., Zhang, H.Y., Wang, S.J., et al., 2011. Multiphase timing of hominin occupations and the paleoenvironment in Luonan Basin, Central China. Quat. Res. 76 (1), 142–147.
Lu, H.Y., An, Z.S., 1997. Paleoclimatic significance of grain size composite of loess deposit in Luochuan. Chin. Sci. Bull. 42 (1), 66–69 (in Chinese).
Lü, H.Y., Han, J.M., Wu, N.Q., Guo, Z.T., 1994. Magnetic susceptibility of modern soils in China and its paleoclimatic implications. Sci. China, Ser. B 24 (12), 1290–1297 (in Chinese).
Lu, H.Y., Zhuo, H.X., Zhang, W.C., Wang, S.J., Zhang, H.Y., Sun, X.F., Jia, X., Xu, Z.W., Wang, X.Y., 2017. Earth surface processes and their effects on human behavior in monsoonal China during the Pleistocene-Holocene epochs. J. Geogr. Sci. 27, 1311–1324.

Lu, Y., Sun, X.F., Xu, X.M., Liu, Y.L., Yi, S.W., 2020. Luminescence dating of reticulated red clay buried in Lanshanmiao paleolithic site in Zhejiang Province, southern China. J. Geogr. Sci. 30 (9), 1436–1450.
Lupien, R.L., Russell, J.M., Grove, M., Beck, C.C., Feibel, C.S., Cohen, A.S., 2020. Abrupt climate change and its influences on hominin evolution during the early Pleistocene in the Turkana Basin, Kenya. Quat. Sci. Rev. 245, 106531.
Lupien, R.L., Russell, J.M., Pearson, E.J., Castañeda, I.S., Asrat, A., Foerster, V., Lamb, H. F., Roberts, H.M., Schäbitz, F., Trauth, M.H., Beck, C.C., Feibel, C.S., Cohen, A.S., 2022. Orbital controls on eastern African hydroclimate in the Pleistocene. Sci. Rep. 12, 3170.
Martinon-Torres, M., Cai, Y.J., Tong, H.W., Pei, S.W., Xing, S., de Castro, J.M., Wu, X.J., Liu, W., 2021. On the misidentification and unreliable context of the new "human teeth" from Fuyan Cave (China). Proc. Natl. Acad. Sci. U.S.A. 118 (22), e2102961118.
Mejdahl, V., Bøtter-Jensen, L., 1994. Luminescence dating of archaeological materials using a new technique based on single aliquot measurements. Quat. Sci. Rev. 13, 551–554.
Moncel, M.-H., Arzarello, M., Boëda, É., et al., 2018. Assemblages with bifacial tools in Eurasia (second part). What is going on in the East? Data from India, Eastern Asia and Southeast Asia. C. R. Palevol 17, 61–76.
Murray, A.S., Marten, R., Johnston, A., Martin, P., 1987. Analysis for naturally occurring radionuclides at environmental concentrations by gamma spectrometry. J. Radioanal. Nucl. Chem. 115, 263–288.
Murray, A.S., Arnold, L.J., Buylaert, J.P., Guérin, G., Qin, J.T., Singhvi, A.K., Smedley, R., Thomsen, K.J., 2021. Optically stimulated luminescence dating using quartz. Nat. Rev. Methods Primers 1, 72.
Murray, A.S., Wintle, A.G., 2003. The single aliquot regenerative dose protocol: potential for improvements in reliability. Radiat. Meas. 37, 377–381.
Nesbitt, H.W., Young, G.M., 1982. Early Proterozoic climates and plate motions inferred from major element chemistry of lutites. Nature 299 (5885), 715–717.
O'Leary, M.H., 1988. Carbon Isotopes in photosynthesis: fractionation techniques may reveal new aspects of carbon dynamics in plants. Bioscience 38, 328–336.
Parker, A., 1970. An index of weathering for silicate rocks. Geol. Mag. 107 (6), 501–504.
Paterson, G.A., Heslop, D., 2015. New methods for unmixing sediment grain size data. G-cubed 16 (12), 4494–4506.
Pei, S.W., 2014. A general review of Oldowan technological classification systems. Acta Anthropol. Sin. 33 (3), 329–342 (in Chinese with English abstract).
Pei, S.W., Gao, X., Wu, X.Z., Li, X.L., Bae, C.J., 2013. Middle to late Pleistocene hominin occupation in the three gorges region, South China. Quat. Int. 295, 237–252.
Porat, N., Duller, G.A.T., Roberts, H.M., Wintle, A.G., 2009. A simplified SAR protocol for TT-OSL. Radiat. Meas. 44, 538–542.
Potts, R., Behrensmeyer, A.K., Faith, J.T., Tryon, C.A., Brooks, A.S., Yellen, J.E., Deino, A. L., Kinyanjui, R., Clark, J.B., Haradon, C.M., Levin, N.E., Meijer, H.J.M., Veatch, E. G., Owen, R.B., Renaut, R.W., 2018. Environmental dynamics during the onset of the Middle Stone Age in eastern Africa. Science 360, 86–90.
Potts, R., Dommain, R., Moerman, J.W., Behrensmeyer, A.K., Deino, A.L., Riedl, S., Beverly, E.J., Brown, E.T., Deocampo, D., Kinyanjui, R., Lupien, R., Owen, R.B., Rabideaux, N., Russell, J.M., Stockhecke, M., de Menocal, P., Faith, J.T., Garcin, Y., Noren, A., Scott, J.J., Western, D., Bright, J., Clark, J.B., Cohen, A.S., Keller, C.B., King, J., Levin, N.E., Shannon, K.B., Muiruri, V., Renaut, R.W., Rucina, S.M., Uno, K., 2020. Increased ecological resource variability during a critical transition in hominin evolution. Sci. Adv. 6, c8975.
Prescott, J.R., Hutton, J.T., 1994. Cosmic ray contributions to dose rates for luminescence and ESR dating: large depths and long-term time variations. Radiat. Meas. 23, 497–500.
Qin, Z.Y., Sun, X.F., 2023. Glacial-Interglacial cycles and early human evolution in China. Land 12, 1683.
Rao, Z.G., Chen, F.F., Zhang, X., Xu, Y.B., Xue, Q., Zhang, P.Y., 2012. Spatial and temporal variations of C3/C4 relative abundance in global terrestrial ecosystem since the Last Glacial and its possible driving mechanisms. Chin. Sci. Bull. 57, 4024–4035.
Rao, Z.G., Jia, G.D., Zhu, Z.Y., Wu, Y., Zhang, J.W., 2008. Comparison of the carbon isotope composition of total organic carbon and long-chain *n*-alkanes from surface soils in eastern China and their significance. Chin. Sci. Bull. 53 (24), 3921–3927.
Rees-Jones, J., 1995. Optical dating of young sediments using fine-grain quartz. Ancient TL 13 (2), 9–14.
Richter, D., Grün, R., Joannes-Boyau, R., Steele, T., Amani, F., Rué, Fernandes, M., Raynal, J.P., Geraads, D., Ben-Ncer, A., Hublin, J., McPherron, S.P., 2017. The age of the hominin fossils from Jebel Irhoud, Morocco, and the origins of the middle stone age. Nature 546, 293–296.
Roberts, R.G., Jacobs, Z., Li, B., Jankowski, N.R., Cunningham, A.C., Rosenfeld, A.B., 2015. Optical dating in archaeology: thirty years in retrospect and grand challenges for the future. J. Archaeol. Sci. 56, 41–60.
Schick, K.D., 1994. The Movius Line reconsidered: perspectives on the earlier paleolithic of eastern Asia. In: Corruchini, R.S., Ciochon, S. (Eds.), Integrative Paths to the Past: Paleoanthropological Advances in Honor of F. clark Howell. Prentice Hall, Upper Saddle River, pp. 569–594.
Schmidt, C., B′osken, J., Kolb, T., 2018. Is there a common alpha-efficiency in polymineral samples measured by various infrared stimulated luminescence protocols? Geochronometria 45, 160–172.
Semaw, S., Rogers, M., Stout, D., 2009. The Oldowan-Acheulian transition: is there a "Developed Oldowan" artifact transition? In: Camps, M., Chauhan, P. (Eds.), Sourcebook of Paleolithic Transitions. Springer Science Business Media, LLC, pp. 173–193.
Shen, G.J., Fang, Y.S., Bischoff, J.L., Feng, Y.X., Zhao, J.X., 2010. Mass spectrometric U-series dating of the Chaoxian hominin site at Yinshan, eastern China. Quat. Int. 211 (1–2), 24–28.
Shipton, C., 2023. Miniaturization and abstraction in the later stone Age. Biological Theory 18, 253–268.
Singarayer, J.S., Bailey, R.M., 2003. Further investigations of the quartz optically stimulated luminescence components using linear modulation. Radiat. Meas. 37, 451–458.
Spooner, N.A., 1994. The anomalous fading of infrared stimulated luminescence from feldspar. Radiat. Meas. 23, 625–632.
Stevens, T., Buylaert, J.P., Murray, A.S., 2009. Towards development of a broadly-applicable SAR TT-OSL dating protocol for quartz. Radiat. Meas. 44, 639–645.
Sun, X.F., Lu, H.Y., Wang, S.J., Yi, S.W., 2012. Ages of liangshan paleolithic sites in hanzhong basin, central China. Quat. Geochronol. 10, 380–386.
Sun, X.F., Wen, S.Q., Lu, C.Q., Zhou, B.Y., Curnoe, D., Lu, H.Y., Li, H.C., Wang, W., Cheng, H., Yi, S.W., Jia, X., Du, P.X., Xu, X.H., Lu, Y.M., Lu, Y., Zheng, H.X., Zhang, H., Sun, C., Wei, L.H., Han, F., Huang, J., Edwards, R.L., Jin, L., Li, H., 2021. Ancient DNA and multimethod dating confirm the late arrival of anatomically modern humans in southern China. Proc. Natl. Acad. Sci. U.S.A. 118 (8), e2019158118.
Thiel, C., Buylaert, J.P., Murray, A.S., Terhorst, B., Hofer, I., Tsukamoto, S., Frechen, M., 2011. Luminescence dating of the Stratzing loess profile (Austria) - testing the potential of an elevated temperature post-IR IRSL protocol. Quat. Int. 234, 23–31.
Tsukamoto, S., Duller, G.A.T., Wintle, A.G., 2008. Characteristics of thermally transferred optically stimulated luminescence (TT-OSL) in quartz and its potential for dating sediments. Radiat. Meas. 43, 1204–1218.
Wallinga, J., Murray, A.S., Duller, G.A.T., Törnqvist, T.E., 2001. Testing optically stimulated luminescence dating of sand-sized quartz and feldspar from fluvial deposits. Earth Planet Sci. Lett. 193, 617–630.
Wallinga, J., Murray, A.S., Wintle, A.G., 2000. The single-aliquot regenerative-dose (SAR) protocol applied to coarse-grain feldspar. Radiat. Meas. 32, 529–533.
Wang, S.J., Lu, H.Y., Zhang, H.Y., Sun, X.F., Yi, S.W., Chen, Y.Y., Zhang, G.K., Xing, L.D., Sun, W.G., 2014a. Newly discovered Paleolithic artefacts from loess deposits and their ages in Lantian, central China. Chin. Sci. Bull. 59, 651–661.
Wang, W., Lycett, S.J., von Cramon-Taubadel, N., Jin, J.J.H., Bae, C.J., 2012. Comparison of Handaxes from Bose Basin (China) and the Western Acheulean Indicates Convergence of Form, Not Cognitive Differences. PLoS One 7 (4), pone.0035804.
Wang, S.J., Sun, X.F., Lu, H.Y., Yi, S.W., Zhang, G.K., Xing, L.D., Zhuo, H.X., Yu, K.F., Wang, W., 2014b. Newly discovered Paleolithic open-air sections in Hanzhong Basin in upper valley of Hanjiang river and their ages. Acta Anthropol. Sin. 33 (2), 125–136 (in Chinese with English abstract).
Wang, W., 2024. Modern human fossils and their ages in southern China. Acta Anthropol. Sin. 43 (6), 934–950 (in Chinese with English abstract).
Wang, W.M., 2022. Phytoliths reveal cycling Pleistocene climate changes at a Paleolithic site in the lower reaches of the Yangtze River, East China. Rev. Palaeobot. Palynol. 306, 104764.
Wang, W., Bae, C.J., Huang, S.M., Huang, X., Tian, F., Mo, J.Y., Huang, Z.T., Huang, C.L., Xie, S.W., Li, D.W., 2014. Middle Pleistocene bifaces from Fengshudao (Bose basin, Guangxi, China). J. Hum. Evol. 69, 110–122.
Wang, X.L., Lu, Y.C., Wintle, A.G., 2006a. Recuperated OSL dating of fine grained quartz in Chinese loess. Quat. Geochronol. 1, 89–100.
Wang, X.L., Lu, Y.C., Wintle, A.G., 2006b. Thermally transferred luminescence in fine-grained quartz from Chinese loess: basic observations. Radiat. Meas. 41, 649–658.
Wang, Y.P., 2017. Late Pleistocene human migrations in China. Curr. Anthropol. 58 (Suppl. 17), 504–513.
Wintle, A.G., Murray, A.S., 2006. A review of quartz optically stimulated luminescence characteristics and their relevance in single aliquot regeneration dating protocols. Radiat. Meas. 41, 369–391.
Wu, X.J., Pei, S.W., Cai, Y.J., Tong, H.W., Li, Q., Dong, Z., Sheng, J.C., Jin, Z.T., Ma, D.D., Xing, S., Li, X.L., Cheng, X., Cheng, H., de la Torre, I., Edwards, R.L., Gong, X.C., An, Z.S., Trinkaus, E., Liu, W., 2019. Archaic human remains from Hualongdong, China, and Middle Pleistocene human continuity and variation. Proc. Natl. Acad. Sci. U.S.A. 116 (20), 9820–9824.
Xie, G.M., Lin, Q., Wu, Y., Hu, Z.H., 2020. The Late Paleolithic industries of southern China (Lingnan region). Quat. Int. 535, 21–28.
Xiong, S.F., Sun, D.H., Ding, Z.L., 2002. Aeolian origin of the red earth in southeast China. J. Quat. Sci. 17 (2), 181–191.
Xu, C.H., Zhang, Y.Y., Chen, C.D., Fang, D.S., 1984. Human occipital bone and mammalian fossils from Chaoxian, Anhui. Acta Anthropol. Sin. 3 (3), 202–209 (in Chinese with English abstract).
Xu, C.H., Zhang, Y.Y., Fang, D.S., 1986. Human fossil newly discovered at Chaoxian, Anhui. Acta Anthropol. Sin. 5 (4), 305–310 (in Chinese with English abstract).
Xu, X.M., 2008. The Paleolithic site survey in Lin'an County. Acta Anthropol. Sin. 27 (1), 38–44 (in Chinese with English abstract).
Xu, X., Zhang, S.W., Zhou, S., 1987. A preliminary study of the vegetation, climate and environment from Wuhu to Jiangyin region since 30000 years B.P. J. Nanjing University 23 (3), 556–574 (In Chinese with English abstract).
Xu, X., Zhu, M.L., 1984. The vegetational and climatic changes in the Zhenjiang region since 15000 years B.P. Acta Geogr. Sin. 39 (3), 277–284 (In Chinese with English abstract).
Yang, H., Xia, Y.F., Zhao, Q.G., Li, X.P., 1995. The character of magnetic susceptibility of red earth profile in South China and palaeo-climate changes. Acta Pedol. Sin. 32 (Suppl. 2), 195–200.

Yang, H., Zhao, Q.G., Li, X.P., Xia, Y.F., 1996. ESR dating of eolian sediment and red earth series from Xuancheng profile in Anhui Province. Acta Pedol. Sin. 33 (3), 293–300 (in Chinese with English abstract).
Yan, W.X., Lu, C.Q., Guo, X.Q., Qin, Z.Y., Cao, Y.K., Sun, X.F., 2024. Chronological study of Luohansi and Yuejiawan open-air paleolithic sites in the lower reaches of the Hanjiang River. J. Earth Sci. Environ. 15 (2), 235–248 (in Chinese with English abstract).
Yang, S.X., Petraglia, M., Deng, C.L., 2024. Human history and behavioral adaptations in North China during marine isotope stage 3. Chin. Sci. Bull. 69, 4257–4266 (in Chinese with English abstract).
Yang, S.X., Yue, J.P., Zhou, X.Y., Storozum, M., Huan, F.X., Deng, C.L., Petraglia, M.D., 2020. Hominin site distributions and behaviours across the Mid-Pleistocene climate transition in China. Quat. Sci. Rev. 248, 106614.
Yang, X.D., Wang, S.M., 1996. Character of palynology and changes of monsoon climate over the last 10000 years in Gucheng Lake, Jiangsu Province. Acta Bot. Sin. 38 (7), 576–581 (In Chinese with English abstract).
Yang, X.Q., Wei, G.J., Yang, J., Jia, G.D., Huang, C.C., Xie, L.H., Huang, W.Y., Argyrios, K., 2014. Paleoenvironmental shifts and precipitation variations recorded in tropical maar lake sediments during the Holocene in Southern China. Holocene 24, 1216–1225.
Yi, S.W., Buylaert, J.P., Murray, A.S., Lu, H.Y., Thiel, C., Zeng, L., 2016. A detailed post-IR IRSL dating study of the niuyangzigou loess site in northeastern China. Boreas 45, 644–657.
Yi, S.W., Li, X.S., Han, Z.Y., Lu, H.Y., Liu, J.F., Wu, J., 2018. High resolution luminescence chronology for Xiashu Loess deposits of Southeastern China. J. Asian Earth Sci. 155, 188–197.
Yi, S.W., Lu, H.Y., Stevens, T., 2012. SAR TT-OSL dating of the loess deposits in the Horqin dunefield (northeastern China). Quat. Geochronol. 10, 56–61.
Yi, S.W., Zeng, L., Xu, Z.W., Wang, Y., Wang, X.Y., Wu, J., Lu, H.Y., 2022. Sea-level changes in the Bohai Sea, northern China, constrained by coastal loess accumulation over the past 200 ka. Quat. Sci. Rev., 107368
Zhan, S.J., Dong, Z., 2023. Stone artifacts discovered during the 2018-2022 Paleolithic surveys in the Shuiyangjiang River Basin, Anhui Province. Acta Anthropol. Sin. 42 (4), 523–530 (in Chinese with English abstract).
Zhan, S.J., Dong, Z., Yi, S.W., 2025. Production and processing of large flakes by hominins during the Middle to Late Pleistocene in the Chaohu Lake Region, Anhui Province. Acta Anthropol. Sin. 44 (5), 874–883 (in Chinese with English abstract).
Zhan, S.J., Dong, Z., Yi, S.W., Zhang, H.Y., Li, H., Pei, S.W., 2022. The stone artifacts discovered in the Paleolithic survey in the Chaohu Lake Region, Anhui Province in 2019. Acta Anthropol. Sin. 41 (5), 927–935 (in Chinese with English abstract).
Zhang, J.F., Li, Y.Y., Han, Y.S., Wang, J.K., 2019. Luminescence dating of weathered sediments from the Paleolithic site of Fengshuzui in northern Hunan province, China. Quat. Geochronol. 49, 211–217.
Zhang, J., Yuan, B., Zhou, L., 2008. Luminescence chronology of "old red sand" in Jinjiang and its implications for optical dating of sediments in South China. Chin. Sci. Bull. 53 (4), 591–601.
Zhang, S.S., Gao, X., Xu, X.M., 2003. First time discovery of Paleolithic remains in Zhejiang Province. Acta Anthropol. Sin. 22 (2), 105–119 (in Chinese with English abstract).
Zhang, S.S., Xu, X.M., Qiu, H.L., Wang, E.L., Luo, Z.G., 2004. A study of stone artifacts found from the Shangmakan Paleolithic site in Anji County, Zhejiang Province. Acta Anthropol. Sin. 23 (4), 264–280 (in Chinese with English abstract).
Zhang, S.S., 1999. On the important advancements of the paleolithic archaeology in China since 1949. Acta Anthropol. Sin. 18 (3), 193–214 (in Chinese with English abstract).
Zhao, J.X., Hu, K., Collerson, K.D., Xu, H.K., 2001. Thermal ionization mass spectrometry U-series dating of a hominid site near Nanjing, China. Geology 29, 27–30.
Zhao, Q.G., Yang, H., 1995. A preliminary study of red earth and changes of quaternary environment in south China. Quat. Sci. 15 (2), 107–116 (in Chinese with English abstract).
Zhao, W.J., Jia, Z.X., Li, S.L., Li, H., 2023. A report of the 2020 excavation of the Shanghu Paleolithic site in Gaoan City, Jiangxi Province. Acta Anthropol. Sin. 42 (3), 373–380 (in Chinese with English abstract).
Zhuo, H.X., Lu, H.Y., Wang, S.J., Ahmad, K., Sun, W.F., Zhang, H.Y., Yi, S.W., Li, Y.X., Wang, X.Y., 2016. Chronology of newly-discovered Paleolithic artifact assemblages in Lantian (Shaanxi province), central China. Quat. Res. 86, 316–325.
Lai, H.C., Zhang, J.F., Li, Y.Y., Zhou, L.P., 2021a. Origin and provenance of Red Clay in north Hunan Province, China: Inferred from grain-size analysis and end-member modelling. Aeolian Res. 51,100714.